PAPER

Exploring the interplay of electron density distribution and electrostatic potential in the interaction of nilutamide and flutamide with androgen receptors using quantum crystallography

Hemalatha Balasubramanian,[a] Kumaradhas Poomani, [ID] *[b] Saravanan Kandasamy,[c] Venkatesha R. Hathwar[d] and Rajesh G. Gonnade[e]

Prostate cancer is a malignant disease commonly found in men. Androgens support the growth and survival of prostate cancer cells. To control this growth and the spread of cancer cells, anti-androgen drugs are necessary to block androgen activity. Effective blocking of androgens depends mainly on the structure, intermolecular interactions and charge density distribution, electrostatic potential (ESP) and binding affinity of drug molecules. Nilutamide (NIL) and flutamide (FLU) are two structurally related non-steroidal anti-androgen drugs (NSAAs) which exhibit serious side effects. The present study explores the charge density distribution, electrostatic potential and intermolecular interactions of NIL and FLU determined from a high-resolution X-ray diffraction experiment and a solid-state quantum chemical theoretical study. Topological analysis of charge density reveals the electron density at the bond critical points of chemical bonds and intermolecular interactions. The electrostatic potential derived from the charge density distribution of both molecules in the crystal has been mapped, which allows a prediction of how the electrostatic interactions, hydrogen bonds, and van der Waals forces govern the binding of these two drug molecules with the androgen receptor at the electronic level. The ESP of interacting groups of both molecules in the androgen active site is approximated to the ESP of those groups in the crystals. The charge density distribution and the electrostatic potential of both molecules were compared. The difference in charge density is reflected in the ESP of NO_2, CF_3 and NH groups and the aromatic ring of both molecules, which is important for drug binding, metabolic stability and toxicity. A molecular docking simulation of both molecules with androgen receptors shows the difference in interactions and binding affinity in the binding pocket of the androgen receptor. The results of the high-resolution X-ray experiment and the advanced computational charge density study of NIL and FLU allows us to understand drug binding and is useful to relate their differing biological effects and toxicities at the electronic level. This information pertains to the design of a new potential androgen inhibitor with improved binding affinity and fewer side effects.

1 Introduction

Cancer is a group of several diseases, which are generally caused by the uncontrolled growth and spread of abnormal cells. In particular, prostate cancer is one of the most commonly diagnosed malignancies worldwide and it is the 6th leading cause of cancer-related death and is commonly found in men.[1] There are several factors that may cause prostate cancer; although the exact cause of prostate cancer is not fully understood, it develops due to DNA changes in prostate cells that cause them to grow uncontrollably. Reports outline that it may be due to radiation, chemical exposure, or genetic mutations.[2,3] Currently, there is no single specific test to diagnose prostate cancer, and the symptoms often do not appear until the disease reaches an advanced stage.[4] Hence, the failure of therapy at this stage is one of the main factors leading to an increased mortality rate.[2] Androgens (male sex hormones) are the primary supporters of the growth and survival of prostate cancer cells. To control the spread of these cancer cells and to reduce the effect of prostate cancer, anti-androgen drugs are being used for treatment.[5] They generally work by blocking androgen activity in the body. Anti-androgens are basically classified into

[a]*Laboratory of Biocrystallography and Computational Molecular Biology, Department of Physics, Periyar University, Salem-636 011, India*

[b]*Department of Physics, Saveetha Engineering College, Chennai-602 105, India. E-mail: kumaradhas@yahoo.com*

[c]*Faculty of Chemistry, University of Warsaw, Poland*

[d]*School of Physical and Applied Sciences, Goa University, Goa-403 206, India*

[e]*Physical and Materials Chemistry Division, CSIR-National Chemical Laboratory, Pune-411 008, India*

steroidal and non-steroidal. Nilutamide (NIL) and flutamide (FLU) are structurally related first-generation non-steroidal anti-androgen drugs (NSAAs) that block androgen activity. Both drugs are used for prostate cancer therapy, but they exhibit several side effects—including hepatotoxicity such as liver damage. In particular, FLU causes significant damage to the liver compared to NIL. Furthermore, NIL causes interstitial pneumonitis; that is, it worsens the lung condition of cancer patients, increasing difficulty in breathing, coughing and chest pain.[6] Both drugs exhibit gastrointestinal issues[7] and common problems—such as hot flushes, visual disturbance, and fluid retention—also worsen the cardiovascular condition of patients. Therefore, to minimize side effects and enhance medicinal activity, androgens should be effectively blocked.[8]

Several methods have been adopted to block androgen activity. Drug delivery to the target is a remarkable technique that is also being studied for cancer treatments that block androgen activity. A recent NMR spectrometric study determined the partition coefficients of NIL and FLU in a lipid nano-emulsion (LNE) to predict the encapsulation efficiency of these drugs to effectively deliver drugs to the target.[9] Examining the binding of androgen inhibitors with the androgen receptor reveals the binding affinity and interaction between the inhibitor and the receptor.[10] In the present study, we report the structures of NIL and FLU at the electronic level to understand the interplay between the electron density distribution and the electrostatic potential of both molecules with the androgen receptor using a high-resolution X-ray diffraction experiment, solid-state quantum chemical theory and molecular docking studies. NIL and FLU are structurally related molecules. NIL is an imidazolidione (five-membered) derivative with tri-fluoromethyl and nitro groups attached to a phenyl ring. Whereas FLU is an anilide derivative with trifluoromethyl, nitro and isobutyramide groups. The binding properties depend mainly on the intermolecular interactions, electron density distribution and the electrostatic potential of androgen blockers.[8] Furthermore, it is expected that the amino acids of the active site of the receptor will interact preferentially with the highly electrostatic potential region of the inhibitor; which depends largely on the concentration of electron density at the point of interaction with the inhibitors. Exploring electron density distribution is envisaged to identify the highly electro-positive and negative potential regions of molecules, and these regions are the preferential binding locations of inhibitor molecules binding with proteins.

Charge density analysis of molecules plays an important role in obtaining fine details of molecular structures at the electronic level, like the electron density distribution of molecules and intermolecular interactions, and electrostatic potential. Thanks to advances in X-ray diffractometers and quantum crystallographic techniques,[11] in recent years, the electronic structures of several molecules have been determined, aiming to explore their biological and material properties.[12] Comparing experimental charge density from high-resolution X-ray diffraction with theoretical calculations allows identification of the limitations of each method and a deeper, complementary understanding can be gained of bonding, non-covalent

interactions, and topological and electrostatic properties that are difficult to predict using theory alone. Therefore, here we have carried out both experimental and theoretical studies of NIL and FLU and compared them. The crystal structures of NIL and FLU molecules have already been reported from X-ray diffraction measurements.[13,14] Single crystals of NIL and FLU compounds were grown and high-resolution X-ray diffraction intensity data were measured at low temperatures of 100 and 90 K, respectively. Topological analysis of the electron density and the electrostatic potential of both molecules was determined from the results of multipole model refinement. Both molecules are structurally related; hence their structural and electronic properties were compared. Furthermore, the experimental results were also compared with a solid-state quantum chemical theoretical study. The results of this study allow the molecules to be redesigned to alleviate adverse side effects and enhance the binding affinity of these inhibitors with the androgen receptor to block androgen activity thereby stop the prostate cancer.

2 Materials and methods

2.1 Experimental methods

2.1.1 Preparation of single crystal. Both NIL and FLU compounds (in powder form) were purchased from Sigma Aldrich. The compounds of NIL and FLU molecules were crystallized at room temperature from ethanol and methanol solvents, respectively. Slow evaporation of a supersaturated solution of both compounds yields crystals of sufficient size within four weeks. The thus-formed NIL crystals were colourless and plate shaped, whereas the FLU crystals were green in colour and block shaped. Good-quality single crystals were selected for high-resolution X-ray diffraction intensity measurements.

2.1.2 X-ray diffraction intensity data collection and data processing. The X-ray diffraction intensity data of the NIL crystal was collected from a SuperNova[15] with a HyPix detector fitted diffractometer with a micro-focus Mo Kα X-ray source ($\lambda = 0.71073$ Å). During data collection, the crystal was cooled by liquid nitrogen using an Oxford Cryostream800 system, and the temperature of the crystal was maintained at 100 K. CrysAlisPro[15] software was used for data collection and processing. A total of 132 201 reflections were collected, of which 12 922 reflections were found as unique. Lorentz and polarization corrections and data reduction were performed. The overall completeness of the measured X-ray diffraction data is 99% resolution $(\sin \theta / \lambda)_{max} = 1.12$ Å^{-1}. An empirical absorption correction was carried out using the multi-scan method implemented in SCALE3 ABSPACK[16] software; the calculated absorption coefficient is 0.149 mm^{-1}. After sorting, merging and averaging the data with SORTAV,[17] 6351 unique reflections were obtained. These reflections were used for structure determination and multipole model refinement.

The high-resolution X-ray diffraction intensity data of the FLU crystal was collected using Bruker D8 Venture[18] with a PHOTON III detector single crystal X-ray diffractometer fitted with a micro-focus Mo Kα ($\lambda = 0.71073$ Å) X-ray source. During data collection, the crystal was cooled by liquid nitrogen gas to

a temperature of 90 K using an Oxford Cryostream800, and this temperature was maintained for the entire data collection period. APEX3 software[19] was used for data collection, measuring 4249 frames. All the frames were integrated with the Bruker SAINT software[20] package, giving a total of 105,808 reflections, of which 13 120 were independent. The overall completeness of the data is 99.4% resolution $(\sin \theta/\lambda)_{max} = 1.11$ Å^{-1}. The data was corrected for Lorentz and polarization effects[20] and also corrected for absorption effects using the multi-scan method implemented in SADABS software;[21] the calculated absorption coefficient is 0.144 mm^{-1}. After sorting, merging and averaging the data with SORTAV,[22] 6892 unique reflections were found, all of which were used for structure determination and multipole model refinement.

The crystal structures of NIL and FLU were solved by direct methods using SHELXS97 and refined in the spherical atom approximation based on F^2 using SHELXL97 (ref. 23) incorporated in the WINGX software package.[24] During the refinement, all hydrogen atoms were located from the Fourier difference map and the positional parameters were refined with the isotropic displacement parameters, whereas the non-hydrogen atoms were refined with anisotropic displacement parameters. The experimental data and spherical atom refinement results are presented in Table 1. Fig. 1 shows the ORTEP3 (ref. 24) plots of NIL and FLU molecules with thermal ellipsoid atoms drawn at 50% probability level.
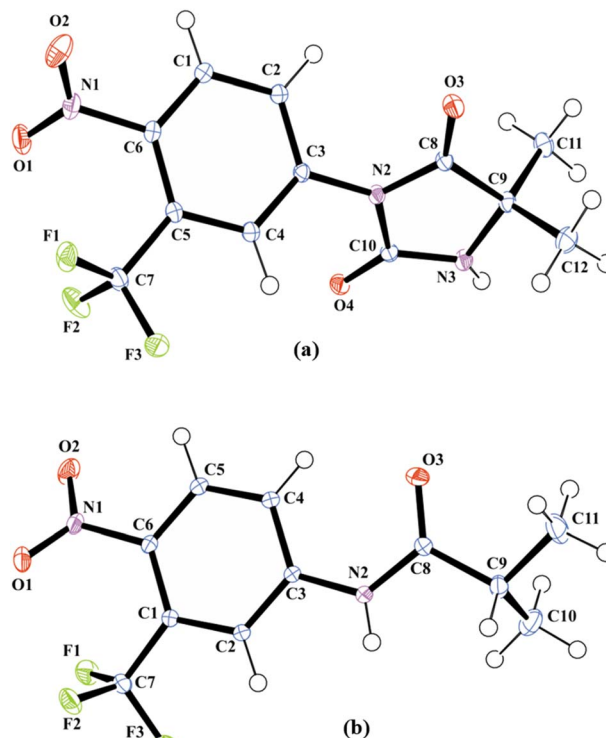

Fig. 1 ORTEP views of (a) NIL and (b) FLU molecules with displacement ellipsoids drawn at the 50% probability level.

Table 1 Crystal data, spherical and multipole refinement details

	Nilutamide	Flutamide
Crystal data and information from X-ray diffraction		
Empirical formula	$C_{12}H_{10}F_3N_3O_4$	$C_{11}H_{11}F_3N_2O_3$
Molecular weight	317.23	276.22
Wavelength (Å)	0.71073	0.71073
Crystal system, space group	Monoclinic, $P2_1/c$	Orthorhombic, $Pna2_1$
Unit cell dimensions (Å, °)	$a = 12.31654(9)$	$a = 11.903(2)$
	$b = 9.83537(7)$	$b = 20.311(4)$
	$c = 12.19673(9)$	$c = 4.8681(8)$
	$\beta = 117.3865(7)$	$\alpha = \beta = \gamma = 90$
Volume (Å^3)	1311.89(2)	1176.9(3)
Z	4	4
Temperature (K)	100	90
Absorption coefficient μ (mm^{-1})	0.149	0.142
F (000)	648	564
Crystal size (mm)	$0.213 \times 0.307 \times 0.376$	$0.09 \times 0.24 \times 0.53$
2θ range for data collection (°)	3.7272 to 53.1617	2.00 to 52.22
Limiting indices	$h = -27$ to 27	$h = -26$ to 26
	$k = -22$ to 22	$k = -45$ to 45
	$l = -27$ to 27	$l = -9$ to 10
Spherical atom refinement		
R_{int}	0.024	0.061
$R(F)$, wR(F^2), S	0.030, 0.0967, 1.033	0.0282, 0.0733, 1.066
No. of reflections used in the refinement	12922	12696
Multipole refinement		
$R(F)$, wR(F^2), S	0.017, 0.041, 1.029	0.0156, 0.0312, 1.1248
No. of reflections used in the refinement	6351	6892
$\Delta\rho_{max}$, $\Delta\rho_{min}$ (eÅ^{-3})	0.112, −0.119	0.199, −0.215

2.1.3 Multipole model refinement. Multipole model refinement of both molecules was carried out with the XDLSM module incorporated in the XD2016 program suite.[25] The Hansen and Coppens multipole formalism[26] was used in this module, in which the electron density of an atom (eqn (1)) is partitioned as:

$$\rho_{atom} = P_c\rho_{core}(r) + P_v K^3\rho_{val}(kr)$$
$$+ \sum_{l=0}^{l_{max}} k'^3 R_l(k'r) \sum_{m=0}^{l} P_{lm\pm}d_{lm\pm}(\theta, \varphi) \qquad (1)$$

where P_c, P_v and P_{lm} are the population parameters, k is the spherical contraction of the valence shell, and k' is the radial expansion and contraction of the valence shell.[26] The second derivative of electron density is the Laplacian of electron density $\nabla^2\rho(r)$ at the critical point (CP). CPs are stationary points in space, where the first derivative of electron density ($\nabla\rho(r) = 0$) is zero. If $\nabla^2\rho(r) < 0$, then the electron density is locally concentrated and if $\nabla^2\rho(r) > 0$, the electron density is locally depleted.[27] The bond critical point (bcp) is located along the bond path between two atoms, where the electron density is a minimum and it is a maximum in all other directions of the bond path.

During the initial stage of multipole refinement, the anisotropic displacement parameters (ADP) of H-atoms of NIL and FLU were obtained from the SHADE3 server,[28] as ADPs provide information about the direction and magnitude of atomic vibrations, offering insights into the flexibility and disorder of the molecule, which is often lost when using only isotropic parameters. The hydrogen ADPs are often difficult to obtain from X-ray diffraction due to their weak scattering; therefore, estimating them is vital for correctly modelling the electron density to interpret the structure of molecules. Then the scale factor was refined to obtain a physically meaningful and accurate model, as it connects the experimental data and the theoretical model. Furthermore, to obtain the accurate positional (x, y, z) and thermal parameters, a high-order refinement was carried out against the data for resolution, $\sin\theta/\lambda > 0.8$ Å^{-1}, which allows the aspherical features of electron density to be correctly modelled. During the high-order refinement, the position of hydrogen atoms was adjusted to the neutron bond lengths (C$_{ar}$–H: 1.083 Å, N–H: 0.967 Å and C$_{sp}^3$–H: 1.059 Å), because the X-ray diffraction data leads to an inaccurate, shortened X–H bond length due to the electron density shifting towards the more electronegative atom. Chemical constraints were imposed on the chemically equivalent atoms and constrained refinement was carried out, in which the P_v, k, and $P_{lm} + k'$ parameters were refined separately until convergence. During this multipole refinement, the fluorine atoms were treated up to hexadecapole level ($l = 4$), whereas all other non-hydrogen atoms were treated up to octupole level ($l = 3$), and all the hydrogen atoms were treated up to dipole level ($l = 2$). The expansion/contraction parameter k for H atoms was fixed at 1.2. This constraint refinement was performed until convergence was attained; then the chemical constraints were removed systematically and unconstrained refinement was carried out. During the unconstrained refinement, P_v, k, $P_{lm} + k'$, scale, and $xyz + U_{ij}$ parameters were refined separately until convergence

was reached. Before this refinement was complete, different model multipole refinements were carried out. Charge neutrality was maintained over the entire refinement. The final refinement results are presented in Table 1. The XDFOUR module of XD2016 was used to generate the residual electron density map. Fig. 5 shows the residual electron density of NIL and FLU molecules. The featureless residual electron density map reveals that there is no significant residual density in the bonding region of the molecule, confirming the correctness of the model. The minimum and maximum residual electron density values of NIL and FLU molecules are −0.112, 0.119 eÅ^{-3} and 0.199, −0.215 eÅ^{-3}, respectively. The results obtained from multipole model refinement were used for topological analysis of electron density.

2.1.4 Calculation of electron density and Laplacian of electron density. To understand the electron density distribution of NIL and FLU molecules, topological analysis of the electron density of both molecules was carried out.[29,30] The electron density is an observable quantity, which is a maximum near the nucleus and a minimum elsewhere;[31] it allows the charge accumulation at the critical point of bond and chemical reactivity[12] of molecules to be understood. A search for the bond critical point (bcp) for both molecules was carried out, which gave a (3, −1) type of critical point for all chemical bonds of both molecules. Topological parameters, such as electron density $\rho_{bcp}(r)$, Laplacian of electron density $\nabla^2\rho_{bcp}(r)$ and other parameters, were determined at the bcp of all bonds (Table 3). Similarly, a (3, −1) type of critical point was also found for all intermolecular interactions reported here, and their topological parameters were also determined (Table 4). Fig. 7(a and b) shows the Laplacian map of electron density of NIL and FLU molecules. The electron density $\rho_{bcp}(r)$, the Laplacian of electron density $\nabla^2\rho_{bcp}(r)$, the ellipticity ε and the eigenvalues (λ_1, λ_2, λ_3) of the Hessian matrix at the bond critical points (bcp) were calculated using the XDPROP module of the XD2016 program suite.[25] Furthermore, energetic properties, such as potential energy density [$G(r)$], kinetic energy density [$V(r)$] and total energy density [$E(r)$], were calculated using the Abramov and Espinosa formulae.[32]

2.2 Computational methods

2.2.1 Solid-state quantum chemical calculation. To validate the results of the topological analysis of electron density of NIL and FLU molecules, we performed a theoretical solid-state quantum chemical calculation using CRYSTAL09 software.[33] To carry out this theoretical calculation, the geometry of both molecules was taken as an input obtained from the experimental multipole refinement. The solid-state periodic quantum chemical calculation was carried out using density functional theory (DFT) B3LYP[34] with the basis set 6-31G**.[35] The shrinking factors (IS1–IS3) along the reciprocal lattice vectors were set at 4 (3 K points in the irreducible Brillouin zone). In the calculation, the truncation parameters were set as ITOL1 – ITOL2 = ITOL3 = ITOL4 = 6 and ITOL5 = 14. To obtain better convergence, the level shifter value was set to 0.6 hartree per cycle. The atomic position and displacement parameters were

fixed at the values obtained from the experiment. Multipolar refinement of the theoretical structure factors was carried out with the same multipoles as were used in the experiment. The calculated topological properties of electron density, Laplacian and other parameters were compared with the results of the experimental study.

2.2.2 Molecular docking simulation. To understand the binding nature of NIL and FLU molecules with the androgen receptor, a molecular docking simulation was carried out. To obtain the complex forms of NIL and FLU molecules with the androgen receptor protein, both molecules were docked into the active site of the androgen receptor protein. Prior to the docking simulation, the geometries of the NIL and FLU molecules were optimized by quantum chemical calculations using GAUSSIAN03 software[36] at the B3LYP/6-311G** level; this energy-minimized geometry of the molecules was used for the molecular docking process. The complex form of the androgen receptor protein was obtained from the RCSB Protein Data Bank (PDB ID: 2ax9)[10] of resolution 1.65 Å and prepared for the molecular docking process. Furthermore, the grid box creation,

polar hydrogens and Gasteiger partial charges were also added with AutoDock Vina tools[37,38] and the target file was saved in pdbqt format. The grid size $25 \times 25 \times 25$ Å was fixed to form a grid box with 0.375 Å grid spacing. Molecular simulation was performed using AutoDock Vina,[37,38] to give a log file, consisting of 10 conformers, which were ranked based on the binding energy values. The essential hydrogen bonding and the other intermolecular interactions were analysed using PyMOL[39] and Discovery studio visualizer[40] packages.

3 Results and discussion

3.1 Intermolecular interactions, Hirshfeld surface and fingerprint plot analysis

The crystal structures of NIL and FLU molecules have already been reported.[13,14] In the present study, we have redetermined the crystal structures of both molecules from X-ray diffraction intensity measurements at low temperatures of 100 and 90 K, respectively. The ORTEP[41] view of both molecules shows the atoms with thermal ellipsoids (Fig. 1). The geometrical
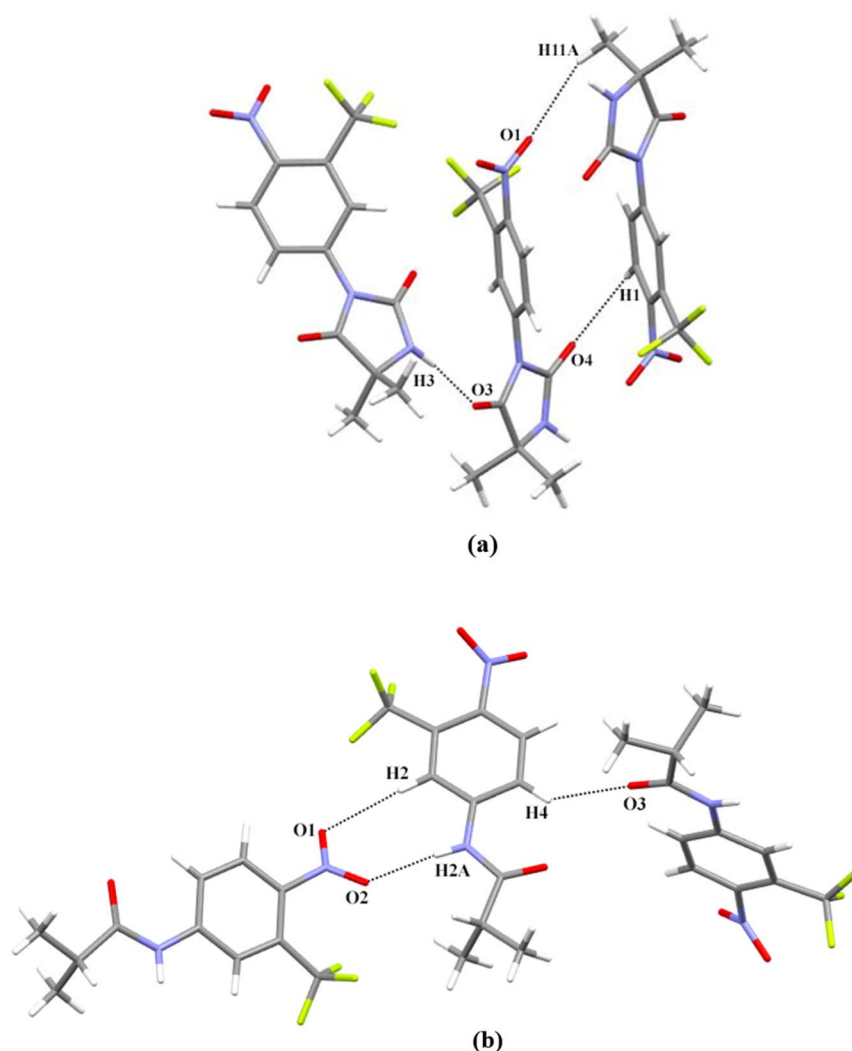

Fig. 2 The hydrogen bonding interactions of (a) NIL and (b) FLU molecules in the crystal.

Table 2 Intermolecular interactions (Å, °) of NIL and FLU molecules

D–H···A	D–H	H···A	D···A	∠D–A···H
Nilutamide[a]				
N3–H3···O3[(i)]	0.903(1)	1.982(1)	2.880(3)	173(1)
C1–H1···O4[(ii)]	0.956(1)	2.542(1)	3.206(4)	126(2)
C11–H11A···O1[(ii)]	0.959(1)	2.597(1)	3.440(5)	146(2)
Flutamide[b]				
N2–H2A···O2[(i)]	0.864(1)	2.193(1)	3.0472(2)	170(1)
C2–H2···O1[(i)]	0.948(1)	2.511(1)	3.4574(3)	176(1)
C4–H4···O3[(ii)]	0.940(1)	2.352(1)	3.0912(2)	135(1)
C11–H11B···O3[(iii)]	1.000(2)	2.580(2)	3.3961(1)	139(1)

[a] Symmetry code: (i) x, $1/2 - y$, $-1/2 + z$, (ii) $1 - x$, $-y$, $-z$. [b] Symmetry code: (i) $-1/2 + x$, $1/2 - y$, $-1 + z$, (ii) $1 - x$, $1 - y$, $1/2 + z$, (iii) x, y, $-1 + z$.

parameters of both molecules were determined and agree with the reported structures.[13,14] The intermolecular interactions were analysed using PLATON[42] and PARST[43] programs incorporated in the WINGX package.[41] Both structures were stabilized by strong and weak intermolecular interactions in the crystal. Fig. 2 shows that the N–H···O and C–H···O types of

interaction form a network with the neighbouring molecules in the crystal. In the NIL molecule, among all the interactions, the N3–H3···O3[(i)] interaction is considered to be the strong hydrogen-bonding interaction. The hydrogen-bonding parameters of the N3–H3···O3[(i)] interaction are N3···O3: 2.880(3) Å and H3···O3:1.982(1) Å and the angle is 173(1)° [symmetry code: (i) x, $1/2 - y$, $-1/2 + z$]. Apart from the above interaction, some very weak C–H···O and C–H···F types of interaction are also found in the crystal. On the other hand, among the interactions of the FLU molecule, the N2–H2A···O2[(i)] and C2–H2···O1[(i)] interactions are considered to be strong interactions. The hydrogen-bonding parameters of the N2–H2A···O2[(i)] interaction are N2···O2: 3.0472(2) Å and H2A···O2: 2.193(1) Å and the angle is 170(1)°; the parameters of the C2–H2···O1[(i)] interaction are C2···O1: 3.457(3) Å and H2···O1: 2.511(1) Å and the angle is 176(1)° [symmetry code: (i) $-1/2 + x$, $1/2 - y$, $-1 + z$]. FLU also exhibits some very weak C–H···O and C–H···F types of interaction in the crystal. The geometrical parameters of all the intermolecular interactions are presented in Table 2.
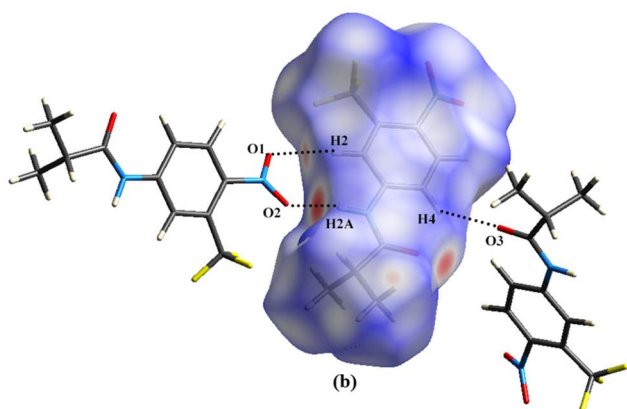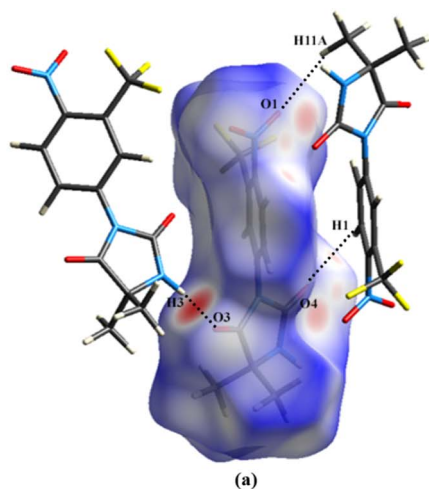

Fig. 3 Hirshfeld surfaces of (a) NIL and (b) FLU molecules.
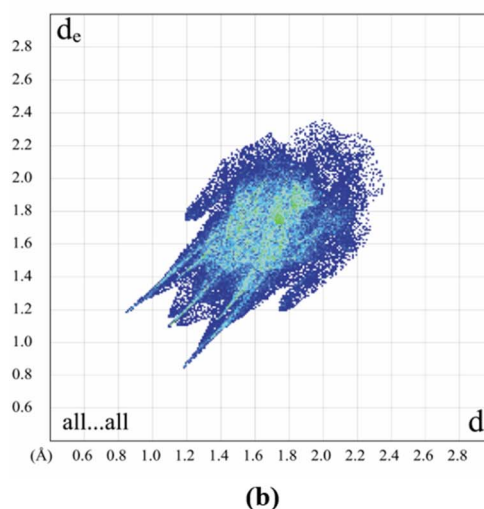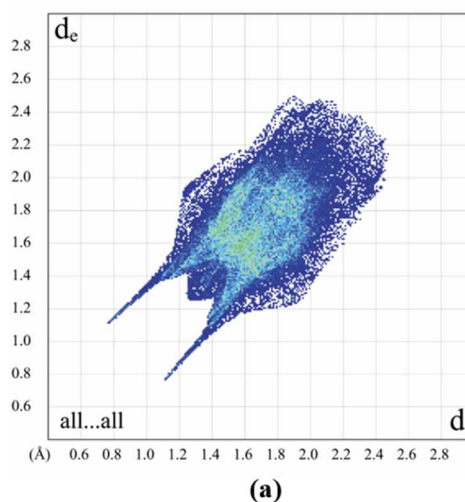

Fig. 4 Fingerprint plots of (a) NIL and (b) FLU molecules.

Intermolecular interactions play an important role in the binding process of molecules in biological targets and materials. To explore the intermolecular interactions, Hirshfeld (HS) surface analysis of molecules is widely used, which allows us to visualize the intermolecular interactions of molecules in the crystal by defining a boundary around the molecule where the electron density of the molecule is dominant. In the present study, the HS surfaces of NIL and FLU molecules were mapped with d_{norm} in the ranges −0.5644 to 0.4387 and −0.4274 to 1.2131, respectively, using CrystalExplorer software.[44] Fig. 3 shows the HS surfaces of NIL and FLU molecules displaying weak and strong interactions with the neighboring molecules; in which the dark red spots around the oxygen atoms of both molecules (Fig. 3(a and b)) indicate the strong hydrogen-bonding nature of the N3–H3···O3$^{(i)}$ and N2–H2A···O2$^{(i)}$ interactions present in the crystals of NIL and FLU molecules, respectively. The white-coloured spots on the surface indicate

contacts that are close to van der Waals radii and the blue-coloured spots show contacts that are longer than van der Waals radii.

A fingerprint plot is a 2D graphical representation, which allows us to analyse intermolecular interactions of different types within a crystal and it is useful for visualizing the frequency of d_i and d_e distances on the Hirshfeld surface. Fig. 4 shows the fingerprint plots of both molecules, giving the percentage contributions of all interactions present in the crystal structure. In the NIL crystal structure, the H···H interaction contributes 17.3% to the total HS, the H···O interaction contributes 29.8% and the F···H interaction contributes 27.8%. In the FLU crystal structure, the H···H interaction contributes 23.5%, the H···O interaction contributes 24.7% and the F···H interaction contributes 25.1%. These interactions make the maximum contribution, and there are interactions present that make minimum contributions in the NIL and FLU crystal
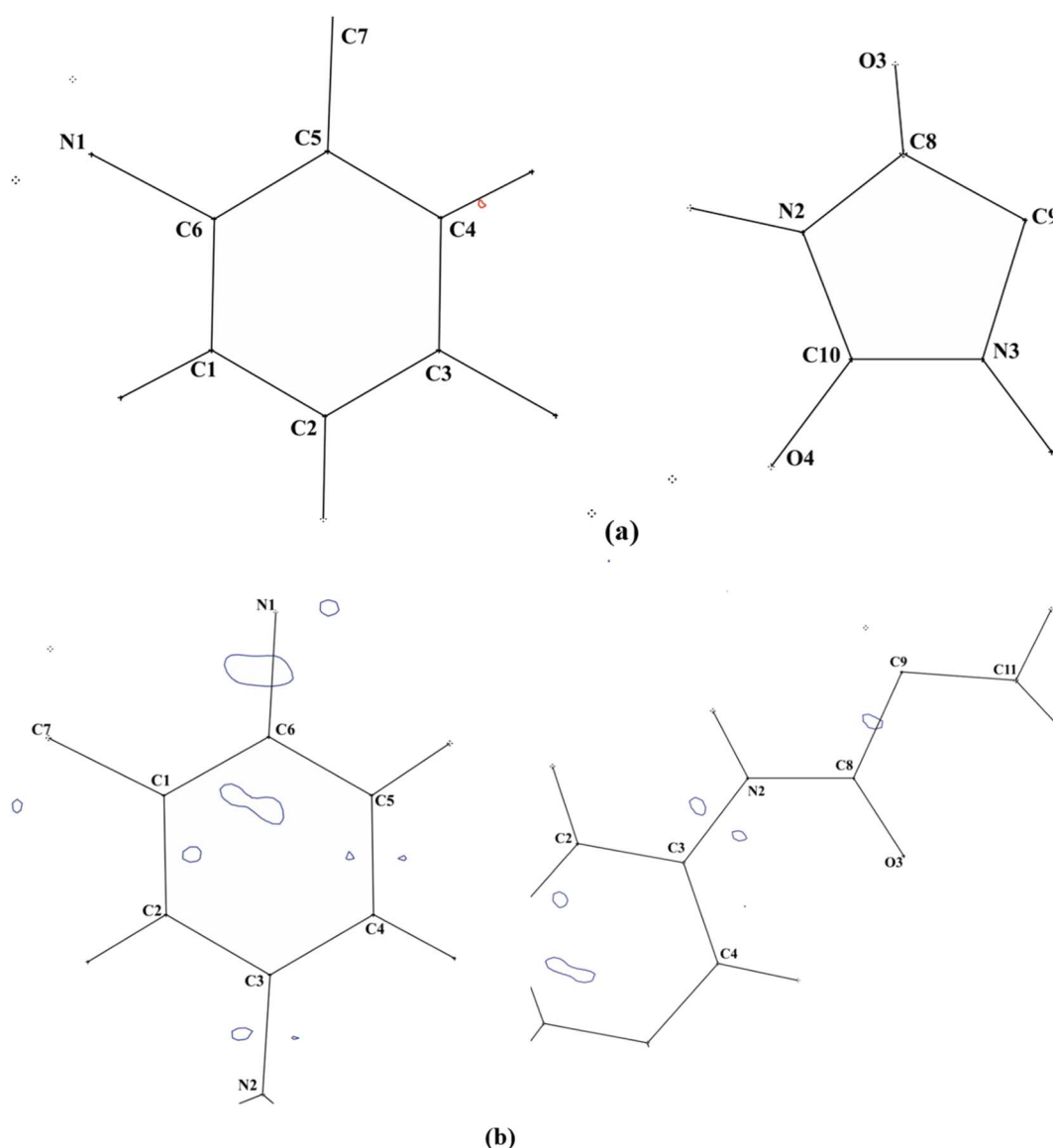

Fig. 5 Residual electron density of (a) NIL and (b) FLU molecules. The contours are drawn at a step size 0.1 eÅ^{-3}.

Table 3 Topological properties of electron density at the bcp of NIL and FLU molecules. First-line values are derived from the experimental data and second-line values are derived from the CRYSTAL09 calculations. R_{ij} is the total bond path length; λ_1, λ_2, and λ_3 are eigenvalues of the Hessian matrix; d_1 and d_2 are the distances between the bcp and each bonded atom; ε is the bond ellipticity

Bond	$\rho_{bcp}(r)$ (eÅ^{-3})	$\nabla^2\rho_{bcp}(r)$ (eÅ^{-5})	R_{ij} (Å)	d_1 (Å)	d_2 (Å)	λ_1 (eÅ^{-5})	λ_2 (eÅ^{-5})	λ_3 (eÅ^{-5})	ε
Nilutamide									
F1–C7	1.927	−16.730	1.3490	0.8329	0.5161	−16.49	−12.99	12.75	0.27
	1.523	−15.580	1.3483	0.8717	0.4766	−15.98	−11.84	12.25	0.35
F3–C7	1.992	−22.050	1.3409	0.8577	0.4832	−17.26	−16.16	11.37	0.07
	1.946	−19.310	1.3409	0.8821	0.4588	−17.09	−15.72	13.50	0.09
F2–C7	1.765	−11.028	1.3375	0.8707	0.4669	−15.26	−10.77	15.01	0.42
	1.705	−8.169	1.3378	0.8866	0.4511	−16.01	−10.80	18.64	0.48
O1–N1	3.322	−12.462	1.2278	0.6457	0.5821	−30.94	−28.00	46.48	0.11
	3.371	−12.228	1.2278	0.6400	0.5878	−30.39	−27.99	46.15	0.09
O2–N1	3.329	−12.916	1.2212	0.6458	0.5754	−30.94	−27.95	45.97	0.11
	3.367	−11.783	1.2213	0.6352	0.5861	−30.21	−27.40	45.83	0.10
O4–C10	3.017	−35.460	1.2135	0.7696	0.4439	−30.24	−25.30	20.09	0.20
	3.048	−35.653	1.2132	0.7645	0.4487	−27.72	−24.61	16.68	0.13
O3–C8	2.982	−35.962	1.2165	0.7731	0.4434	−29.53	−27.31	20.88	0.08
	2.978	−37.430	1.2165	0.7762	0.4403	−30.01	−27.65	20.22	0.09
N2–C8	2.090	−22.098	1.3738	0.8216	0.5522	−16.80	−15.32	10.02	0.10
	2.098	−23.102	1.3736	0.8232	0.5505	−17.22	−15.29	9.41	0.13
N2–C3	1.948	−17.070	1.4158	0.8321	0.5837	−14.85	−13.59	11.37	0.09
	1.932	−16.750	1.4158	0.8323	0.5835	−14.56	−13.67	11.48	0.07
N2–C10	2.099	−21.367	1.4274	0.8379	0.5895	−17.84	−14.83	11.30	0.20
	2.156	−18.010	1.4283	0.8078	0.6205	−17.81	−14.33	14.13	0.24
N3–C10	2.296	−23.906	1.3485	0.7784	0.5701	−21.29	−15.79	13.17	0.35
	2.374	−24.141	1.3484	0.7779	0.5705	−21.08	−15.90	12.84	0.33
N3–C9	1.778	−9.935	1.4640	0.8281	0.6359	−12.36	−11.89	14.31	0.04
	1.806	−10.259	1.4640	0.8354	0.6285	−12.36	−11.95	14.05	0.03
N3–H3	2.176	−27.70	0.9667	0.7294	0.2372	−30.44	−28.43	31.17	0.07
	2.215	−28.282	0.9667	0.7320	0.2346	−30.93	−28.99	31.64	0.07
N1–C6	1.865	−13.264	1.4682	0.8422	0.6259	−13.89	−12.94	13.57	0.07
	1.846	−13.939	1.4681	0.8638	0.6043	−13.73	−12.41	12.21	0.11
C5–C4	2.169	−18.216	1.3907	0.7041	0.6867	−16.43	−13.27	11.48	0.24
	2.157	−17.998	1.3907	0.7005	0.6902	−16.50	−13.27	11.77	0.24
C5–C6	2.122	−17.515	1.3979	0.6713	0.7266	−16.21	−13.05	11.75	0.24
	2.079	−17.565	1.3978	0.6775	0.7203	−16.04	−12.88	11.36	0.25
C5–C7	1.835	−13.027	1.5089	0.7076	0.8013	−13.22	−11.65	11.83	0.13
	1.804	−13.767	1.5089	0.7126	0.7963	−13.37	−11.47	11.07	0.17
C8–C9	1.715	−10.784	1.5272	0.7826	0.7447	−12.02	−10.86	12.09	0.11
	1.747	−11.412	1.5272	0.7841	0.7432	−12.26	−10.88	11.73	0.13
C2–C3	2.162	−18.825	1.3919	0.6692	0.7226	−16.36	−13.24	10.77	0.23
	2.183	−19.250	1.3919	0.6697	0.7223	−16.47	−13.30	10.52	0.24
C2–C1	2.159	−18.998	1.3915	0.7029	0.6887	−16.21	−13.35	10.56	0.21
	2.143	−18.995	1.3916	0.6841	0.7074	−16.24	−13.30	10.54	0.22
C2–H2	1.763	−15.888	1.0833	0.7288	0.3545	−16.84	−16.17	17.13	0.04
	1.793	−16.832	1.0833	0.7260	0.3574	−17.14	−16.48	16.79	0.04
C9–C12	1.619	−9.598	1.5281	0.7877	0.7404	−10.44	−10.30	11.15	0.01
	1.637	−10.301	1.5281	0.7885	0.7396	−10.48	−10.40	10.58	0.01
C9–C11	1.620	−9.704	1.5309	0.8011	0.7298	−10.63	−10.03	10.96	0.06
	1.605	−10.036	1.5310	0.8073	0.7237	−10.49	−9.80	10.25	0.07
C1–C6	2.254	−21.235	1.3850	0.6882	0.6968	−17.78	−14.31	10.86	0.24
	2.236	−21.640	1.3850	0.6895	0.6955	−17.56	−14.33	10.25	0.23
C1–H1	1.805	−16.294	1.0833	0.7093	0.3739	−16.89	−15.63	16.22	0.08
	1.887	−18.066	1.0833	0.6850	0.3982	−17.26	−15.98	15.17	0.08
C4–C3	2.212	−20.630	1.3951	0.6933	0.7018	−17.34	−14.17	10.88	0.22
	2.236	−20.632	1.3951	0.6942	0.7009	−17.39	−14.06	10.82	0.24
C4–H4	1.871	−18.580	1.0832	0.7180	0.3652	−17.85	−17.09	16.36	0.04
	1.896	−18.613	1.0832	0.7196	0.3636	−18.11	−17.34	16.84	0.04
C11–H11A	1.752	−15.004	1.0595	0.7077	0.3518	−16.10	−15.84	16.93	0.02
	1.741	−15.644	1.0595	0.7168	0.3427	−15.86	−15.65	15.86	0.01
C11–H11C	1.744	−16.089	1.0589	0.6872	0.3718	−15.85	−15.55	15.31	0.02
	1.716	−16.139	1.0589	0.7028	0.3561	−15.59	−15.34	14.79	0.02
C11–H11B	1.764	−16.521	1.0595	0.6963	0.3633	−16.23	−15.70	15.40	0.03
	1.736	−16.767	1.0595	0.7107	0.3488	−15.98	−15.48	14.68	0.03

Table 3 (*Contd.*)

Bond	$\rho_{bcp}(r)$ (e$\mathring{A}^{-3}$)	$\nabla^2\rho_{bcp}(r)$ (e$\mathring{A}^{-5}$)	R_{ij} ($\mathring{A}$)	d_1 ($\mathring{A}$)	d_2 ($\mathring{A}$)	λ_1 (e$\mathring{A}^{-5}$)	λ_2 (e$\mathring{A}^{-5}$)	λ_3 (e$\mathring{A}^{-5}$)	ε
C12–H12B	1.680	−14.073	1.0605	0.6830	0.3775	−15.11	−14.31	15.34	0.06
	1.677	−14.884	1.0604	0.7026	0.3578	−15.23	−14.57	14.92	0.05
C12–H12C	1.710	−13.699	1.0584	0.6953	0.3631	−15.27	−14.80	16.37	0.03
	1.715	−14.313	1.0584	0.7209	0.3375	−15.61	−15.26	16.55	0.02
C12–H12A	1.736	−14.193	1.0591	0.7030	0.3561	−15.90	−15.17	16.87	0.05
	1.763	−15.178	1.0592	0.7064	0.3528	−15.90	−15.28	15.99	0.04
Flutamide									
F1–C7	1.885	−10.240	1.3462	0.9139	0.4323	−18.24	−14.82	22.82	0.23
	1.964	−19.898	1.3435	0.8391	0.5043	−15.59	−15.08	10.77	0.03
F2–C7	1.960	−11.734	1.3375	0.9068	0.4307	−18.82	−16.35	23.44	0.15
	1.989	−20.309	1.3361	0.8433	0.4927	−16.29	−14.93	10.91	0.09
F3–C7	1.922	−18.978	1.3509	0.8999	0.4511	−17.62	−14.54	13.19	0.21
	1.945	−19.331	1.3493	0.8453	0.5040	−15.47	−14.67	10.80	0.05
O1–N1	3.266	−9.185	1.2289	0.6301	0.5988	−30.34	−23.33	44.49	0.30
	3.299	−12.173	1.2283	0.6224	0.6059	−28.96	−26.90	43.68	0.08
O2–N1	3.268	−11.424	1.2346	0.6369	0.5977	−30.47	−24.96	44.01	0.22
	3.217	−10.616	1.2345	0.6320	0.6025	−28.49	−25.80	43.91	0.10
O3–C8	2.802	−13.642	1.2179	0.8089	0.4089	−27.19	−23.46	37.01	0.16
	2.861	−21.780	1.2181	0.7973	0.4208	−25.31	−23.15	26.68	0.09
N1–C6	1.655	−14.213	1.4615	0.8964	0.5651	−12.85	−9.42	8.06	0.37
	1.759	−11.985	1.4607	0.8888	0.5719	−11.81	−11.01	10.84	0.07
N2–C3	2.179	−20.073	1.3982	0.7942	0.6040	−17.11	−14.60	11.64	0.17
	2.002	−14.659	1.3976	0.8035	0.5942	−14.74	−13.61	13.70	0.08
N2–C8	2.168	−26.233	1.3823	0.8708	0.5115	−17.01	−14.48	5.26	0.18
	2.109	−20.758	1.3815	0.8227	0.5588	−16.11	−14.53	9.88	0.11
C1–C2	2.069	−19.258	1.3908	0.6653	0.7255	−15.01	−11.37	7.12	0.32
	2.100	−17.007	1.3902	0.6958	0.6944	−15.21	−12.21	10.42	0.25
C1–C6	2.102	−21.811	1.4075	0.7336	0.6739	−16.25	−12.12	6.56	0.34
	2.017	−15.529	1.4075	0.6898	0.7177	−14.37	−11.71	10.55	0.23
C1–C7	1.827	−15.143	1.5143	0.6950	0.8193	−12.50	−11.01	8.37	0.14
	1.758	−11.941	1.5139	0.6877	0.8263	−12.10	−11.12	11.27	0.09
C2–C3	2.233	−23.148	1.4079	0.6779	0.7301	−17.05	−13.49	7.39	0.26
	2.031	−16.349	1.4077	0.7134	0.6943	−14.65	−12.39	10.69	0.18
N2–H2A	2.224	−29.241	0.9970	0.7391	0.2579	−29.14	−27.40	27.29	0.06
	2.242	−25.281	0.9971	0.7413	0.2558	−29.60	−27.97	32.29	0.06
C3–C4	2.139	−21.552	1.4027	0.7618	0.6409	−15.93	−12.63	7.01	0.26
	2.063	−16.181	1.4028	0.7279	0.6749	−14.48	−12.51	10.81	0.16
C4–C5	2.229	−22.204	1.3920	0.6920	0.7000	−15.68	−13.32	6.80	0.18
	2.069	−16.556	1.3919	0.6835	0.7084	−14.74	−12.66	10.85	0.16
C5–C6	2.224	−22.082	1.3876	0.6402	0.7474	−16.66	−12.28	6.86	0.36
	2.104	−17.436	1.3879	0.6767	0.7112	−15.30	−12.58	10.44	0.22
C8–C9	1.684	−12.160	1.5261	0.8345	0.6916	−11.38	−9.43	8.64	0.21
	1.688	−10.754	1.5257	0.8335	0.6922	−10.72	−10.22	10.19	0.05
C9–C10	1.608	−10.048	1.5366	0.7290	0.8076	−10.30	−9.56	9.82	0.08
	1.556	−8.333	1.5366	0.7626	0.7740	−9.79	−9.55	11.01	0.02
C9–C11	1.632	−10.598	1.5278	0.7288	0.7990	−10.42	−9.81	9.64	0.06
	1.613	−9.057	1.5276	0.7611	0.7665	−10.42	−9.83	11.20	0.06
C2–H2	1.845	−18.779	2.1994	1.8654	0.3340	−17.50	−16.42	15.15	0.07
	1.891	−17.980	1.0692	0.7120	0.3572	−17.92	−17.16	17.10	0.04
C4–H4	1.741	−18.293	3.8767	3.5337	0.3431	−16.09	−15.56	13.35	0.03
	1.885	−18.442	1.0776	0.7218	0.3558	−17.64	−17.36	16.56	0.02
C5–H5	1.820	−19.899	2.2284	1.9259	0.3025	−18.14	−17.02	15.25	0.07
	1.797	−15.777	1.0982	0.7252	0.3730	−16.47	−15.93	16.63	0.03
C9–H9	1.746	−16.560	1.0782	0.6915	0.3867	−15.27	−14.34	13.05	0.07
	1.863	−16.263	1.0779	0.6701	0.4079	−15.81	−15.28	14.82	0.03
C10–H10A	1.880	−19.640	1.0741	0.7281	0.3460	−18.66	−17.84	16.85	0.05
	1.828	−15.490	1.0743	0.6947	0.3796	−16.82	−16.30	17.62	0.03
C10–H10B	1.855	−19.156	3.4664	3.0476	0.4189	−15.63	−15.07	11.55	0.04
	1.983	−18.725	1.0416	0.6609	0.3807	−18.31	−17.71	17.30	0.03
C10–H10C	1.807	−14.800	1.0796	0.7274	0.3522	−17.21	−16.38	18.79	0.05
	1.800	−14.859	1.0796	0.6929	0.3867	−16.26	−15.84	17.24	0.03
C11–H11A	1.672	−15.279	1.0388	0.6908	0.3480	−15.41	−14.69	14.82	0.05

Table 3 (Contd.)

Bond	$\rho_{bcp}(r)$ (eÅ^{-3})	$\nabla^2\rho_{bcp}(r)$ (eÅ^{-5})	R_{ij} (Å)	d_1 (Å)	d_2 (Å)	λ_1 (eÅ^{-5})	λ_2 (eÅ^{-5})	λ_3 (eÅ^{-5})	ε
	2.020	−19.524	1.0385	0.6603	0.3782	−18.66	−18.29	17.43	0.02
C11–H11B	1.769	−17.038	1.0445	0.6849	0.3596	−16.33	−15.97	15.26	0.02
	1.998	−20.313	1.0443	0.6840	0.3603	−19.22	−19.00	17.90	0.01
C11–H11C	1.862	−18.756	1.0795	0.7040	0.3756	−16.98	−16.29	14.51	0.04
	1.820	−15.645	1.0784	0.7030	0.3754	−16.97	−16.40	17.72	0.03

structures. However, NIL forms more interactions than FLU, except for the H···H interaction. The fingerprint plots of both molecules are shown in Fig. 4.

3.2 Topological analysis of electron density

3.2.1 Electron density. The electron density $\rho_{bcp}(r)$ values of all the chemical bonds of NIL and FLU molecules are presented in Table 3; in which the first row shows the experimentally calculated electron density at the bcp of the bonds and the second row is the corresponding theoretical electron density. In the NIL molecule, the experimental electron density value of heteronuclear C–F bonds is in the range 1.765–1.992 eÅ^{-3} and the average value is 1.879 eÅ^{-3}; whereas in FLU, the values range from 1.885 to 1.960 eÅ^{-3} and the average value is 1.923 eÅ^{-3}; these values are comparable with the reported values.[45] The electron density values of the N–O bonds of NIL are 3.323 (N1–O1) and 3.329 eÅ^{-3} (N1–O2); these values are slightly higher than those of the N–O bonds of the FLU molecule; the

maximum value is 3.268 eÅ^{-3}. The high value for the electron density of the N–O bonds indicates high charge accumulation of the bonds,[46] which may be due to the high electron density and electronegativity of the O atom. The electron density of the carbonyl bonds C=O of NIL C8=O3 and C10=O4 are 2.982 and 3.017 eÅ^{-3}, respectively; notably, the electron density of C10=O4 is slightly higher than that of the C8=O3 bond; the difference may be attributed to the difference in the environment of C atoms and intermolecular interactions. There are three types of C–N bonds (C6–N1; C3–N2, C8–N2, C10–N2; C10–N3 and C9–N3) existing in the NIL molecule; the electron densities of these bonds range from 1.778 to 2.296 eÅ^{-3} and the average value is 2.013 eÅ^{-3}; whereas the electron density values of the C6–N1, C3–N2 and C8–N2 bonds of FLU are 1.655, 2.179 and 1.684 eÅ^{-3}, respectively, in which the densities of the C6–N1 and C8–N2 bonds are found to be much lower than those of NIL. The electron density of the aromatic ring C_{ar}–C_{ar} bonds of NIL are in the range 2.122 to 2.212 eÅ^{-3} and the average value is

Table 4 The topological properties of the intermolecular interactions of NIL and FLU molecules

Bonds	$\rho_{cp}(r)$ (eÅ^{-3})	$\nabla^2\rho_{cp}(r)$ (eÅ^{-5})	R_{ij} (Å)	λ_1 (eÅ^{-5})	λ_2 (eÅ^{-5})	λ_3 (eÅ^{-5})	d_1 (Å)	d_2 (Å)	$G(r)$ (a.u.)	$V(r)$ (a.u.)	$H(r)$ (a.u.)
Nilutamide[a]											
N3–H3···O3$^{(i)}$	0.141	2.896	2.8811	−0.71	−0.69	4.25	1.2133	1.6678	0.0182	−0.0064	0.0118
	0.130	3.065	2.8811	−0.63	−0.61	4.30	1.6562	1.2249	0.0352	−0.0387	−0.0035
C1–H1···O4$^{(ii)}$	0.055	0.882	2.5236	−0.17	−0.13	0.95	1.4997	1.0239	0.0093	−0.0095	−0.0002
	0.058	0.880	3.2304	−0.18	−0.17	1.23	1.7937	1.4367	0.0096	−0.0101	−0.0005
C11–H11A···O1$^{(ii)}$	0.039	0.616	3.3345	−0.14	−0.12	0.90	1.5092	1.8253	0.0060	−0.0057	0.0003
	0.037	0.614	3.3136	−0.12	−0.11	0.84	1.5099	1.8037	0.0059	−0.0055	0.0004
C1–H1···F1$^{(iii)}$	0.037	0.640	3.3232	−0.13	−0.10	0.84	1.4628	1.8604	0.0061	−0.0056	0.0005
	0.035	0.629	3.3470	−0.12	−0.11	0.85	1.8884	1.4586	0.0058	−0.0051	0.0007
C4–H4···F3$^{(iv)}$	0.024	0.543	2.5728	−0.08	−0.07	0.64	1.5335	1.0393	0.0045	−0.0034	0.0011
	0.030	0.610	3.4933	−0.10	−0.09	0.80	3.4933	2.0296	0.0053	−0.0043	0.0010
Flutamide[b]											
N2–H2A···O2$^{(i)}$	0.059	2.112	3.0511	−0.25	−0.21	2.57	1.7056	1.3455	0.0051	−0.0117	−0.0066
	0.100	2.161	3.0498	−0.46	−0.45	3.07	1.7585	1.2913	0.0103	−0.0018	0.0085
C2–H2···O1$^{(i)}$	0.063	0.974	3.4584	−0.21	−0.21	1.40	2.0397	1.4186	0.0109	−0.0117	−0.0008
	0.046	0.996	3.4583	−0.17	−0.16	1.32	2.0107	1.4476	0.0093	−0.0083	0.0010
C4–H4···O3$^{(ii)}$	0.097	1.385	3.1239	−0.40	−0.33	2.12	1.7817	1.3422	0.0181	−0.0219	−0.0038
	0.079	1.363	3.1116	−0.35	−0.29	2.01	1.7546	1.3570	0.0155	−0.0169	−0.0014
C2–H2···F1$^{(iii)}$	0.025	0.383	3.4240	−0.10	−0.06	0.54	1.8896	1.5344	0.0034	−0.0029	0.0005
	0.022	0.360	3.4082	−0.07	−0.05	0.48	1.8696	1.5386	0.0031	−0.0025	0.0006
C5–H5···F3$^{(iv)}$	0.032	0.506	3.2952	−0.10	−0.09	0.70	1.8043	1.4910	0.0047	−0.0042	0.0005
	0.030	0.500	3.2943	−0.09	−0.08	0.68	1.8117	1.4825	0.0045	−0.0039	0.0006

[a] Symmetry code: (i) $x, -y + 1/2, z - 1/2$, (ii) $-x + 1, -y + 1, -z + 1$, (iii) $-x + 1, y + 1/2, -z + 1/2 + 1$, (iv) $-x + 1, -y, -z + 1$. [b] Symmetry code: (i) $x + 1/2, -y + 1/2 + 1, z - 1$, (ii) x, y, z, (iii) $x, y, z - 1$, (iv) $x - 1/2, -y + 1/2 + 1, z$.

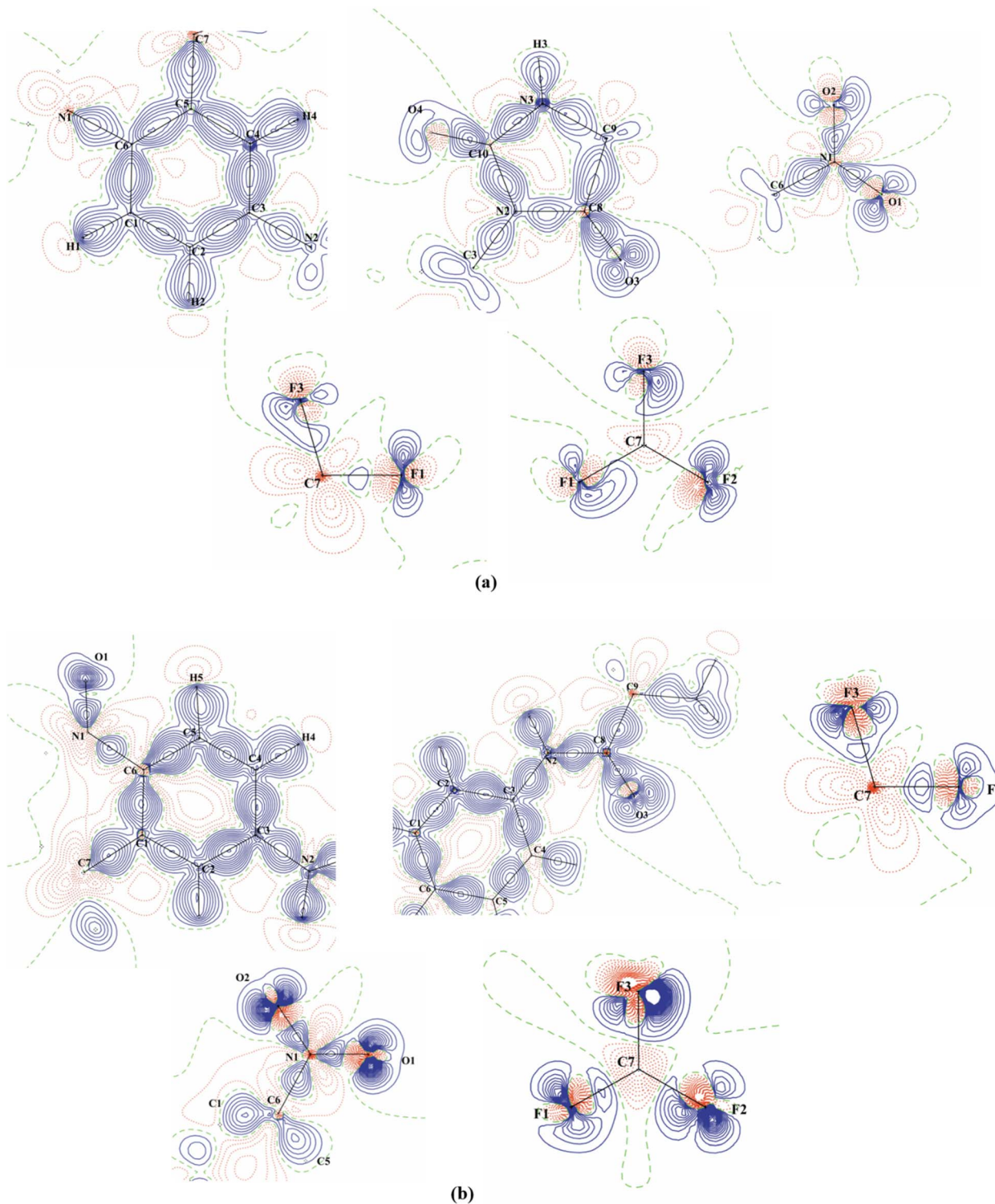**Fig. 6** Experimental deformation density maps of (a) NIL and (b) FLU molecules. Contours are drawn at 0.1 eÅ^{-3} intervals. Solid lines represent positive contours, dotted lines are negative contours and dashed lines are zero contours.

2.179 eÅ^{-3}. A similar trend is also found in the aromatic bonds of the FLU molecule; however, the average electron density of the bonds is 2.159 eÅ^{-3}. Although the aromatic ring of both molecules differs in its attachments, the electron density distribution is not much altered and their average values are

very close and are also comparable with the reported values.[47,48] The electron density of the amino N3–H3 bond of NIL is 2.173 eÅ^{-3}, which is slightly less than the density found in the corresponding N–H bond of FLU, where the value is 2.224 eÅ^{-3}. The density of the C–H bonds of the aromatic and methyl
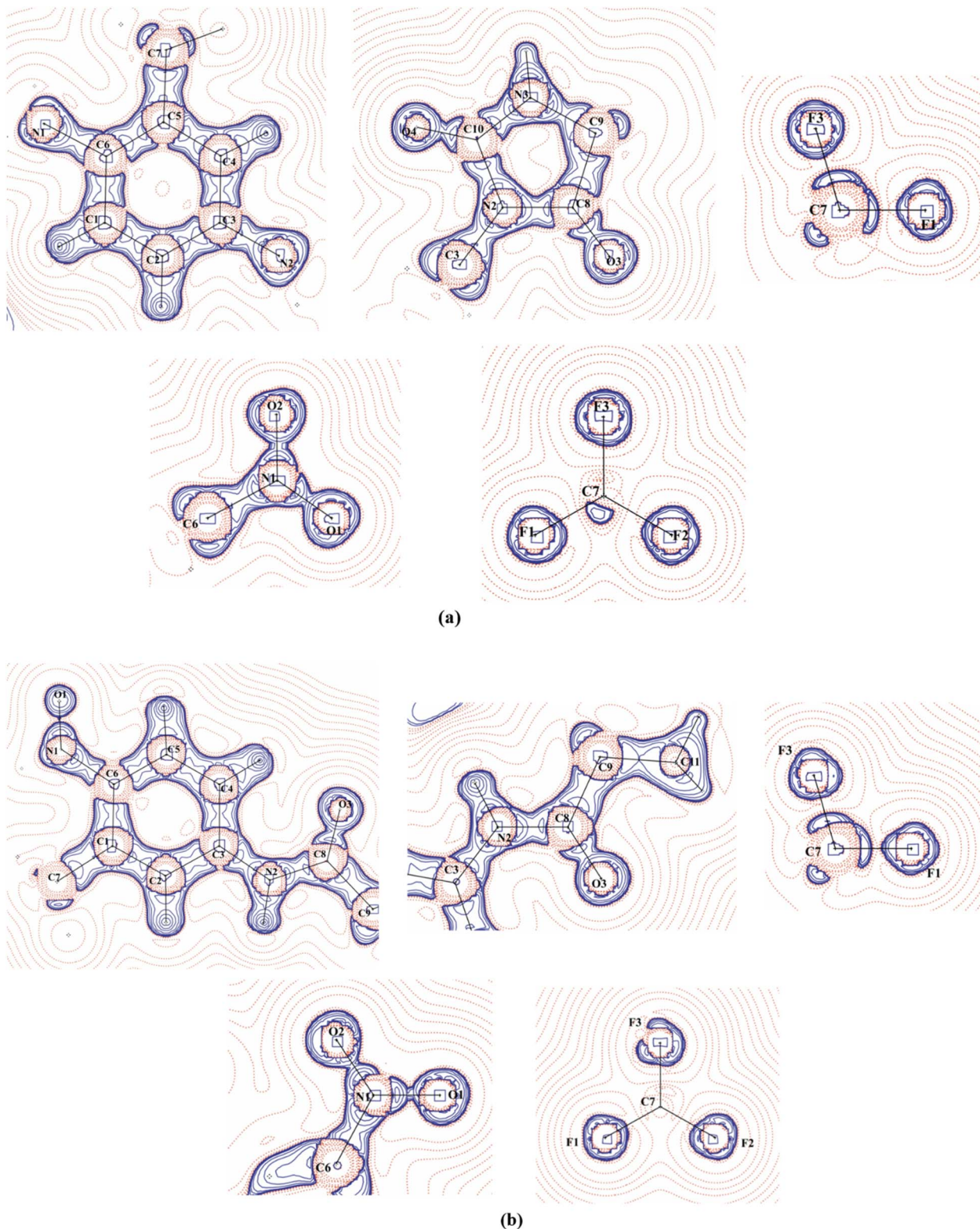
Fig. 7 The Laplacians of electron density of (a) NIL and (b) FLU molecules drawn in the C1, C3, C5 and N2, C8, C10 and N1, O1, O2 planes. Contours are drawn at logarithmic scale, 3×2^N eÅ$^{\pm 5}$ level, where $N = 2$, 4 and 8×10^n, $n = -2$, -1, 0, 1, 2. The solid blue lines indicate the positive contours and dotted red lines are negative contours.

groups of NIL is less than that of the FLU molecule. The charge accumulation in the bonds of non-hydrogen atoms of the NIL molecule is slightly higher than in the FLU molecule, whereas in the N–H and C–H bonds of NIL and FLU, the trend is just the opposite (Table 3).

Fig. 6 shows the deformation electron density maps of NIL and FLU molecules, the lone-pair positions of oxygen and fluorine atoms and the charge accumulation in the bonding regions of the molecules. The bond ellipticity (ε) at the bond critical point (bcp) provides insights into the cylindrical nature and anisotropy of electron density.[49] It also provides information about the π and σ bond nature of the chemical bonds of the molecule. In NIL, the bond ellipticity of C_{ar}–C_{ar} bonds ranges from 0.21 to 0.24 and the average value is 0.23; this value is almost a match with the reported ellipticity of aromatic bonds.[50] Whereas in the FLU molecule, the ellipticity of C_{ar}–C_{ar} bonds is relatively higher than that of the NIL bonds and the maximum value is 0.36.[51] The ellipticities of the C–F bonds of both molecules are not comparable, and the values differ; this may be due to their interaction with their neighbours.

3.2.2 Laplacian of electron density.

In the NIL molecule, the experimental Laplacian values of C–F bonds are unequal; the value ranges from -11.028 to -22.05 eÅ^{-5}. The same trend is also found in FLU; however, the Laplacian values are found to be a little lower, the maximum value is -18.978 eÅ^{-5}. The difference in Laplacian values indicates that the charges of the C–F bonds of FLU are less concentrated than in the NIL molecule. The Laplacians of the N–O bonds of NIL are almost equal and the values are -12.462 (N1–O1) and -12.916 eÅ^{-5} (N1–O2); whereas in FLU molecules, these values are found to be lower and the maximum Laplacian value is -11.424 eÅ^{-5}. Relief maps [Fig. 8(a and b)] of the negative Laplacians of the electron density of the NO$_2$ and CF$_3$ groups of NIL and FLU molecules display the lone-pair lobes of O and F atoms of both groups. The Laplacians of the C_{ar}–C_{ar} bonds of NIL range from -17.515 to -21.235 eÅ^{-5}; the large variation in the Laplacian is attributed

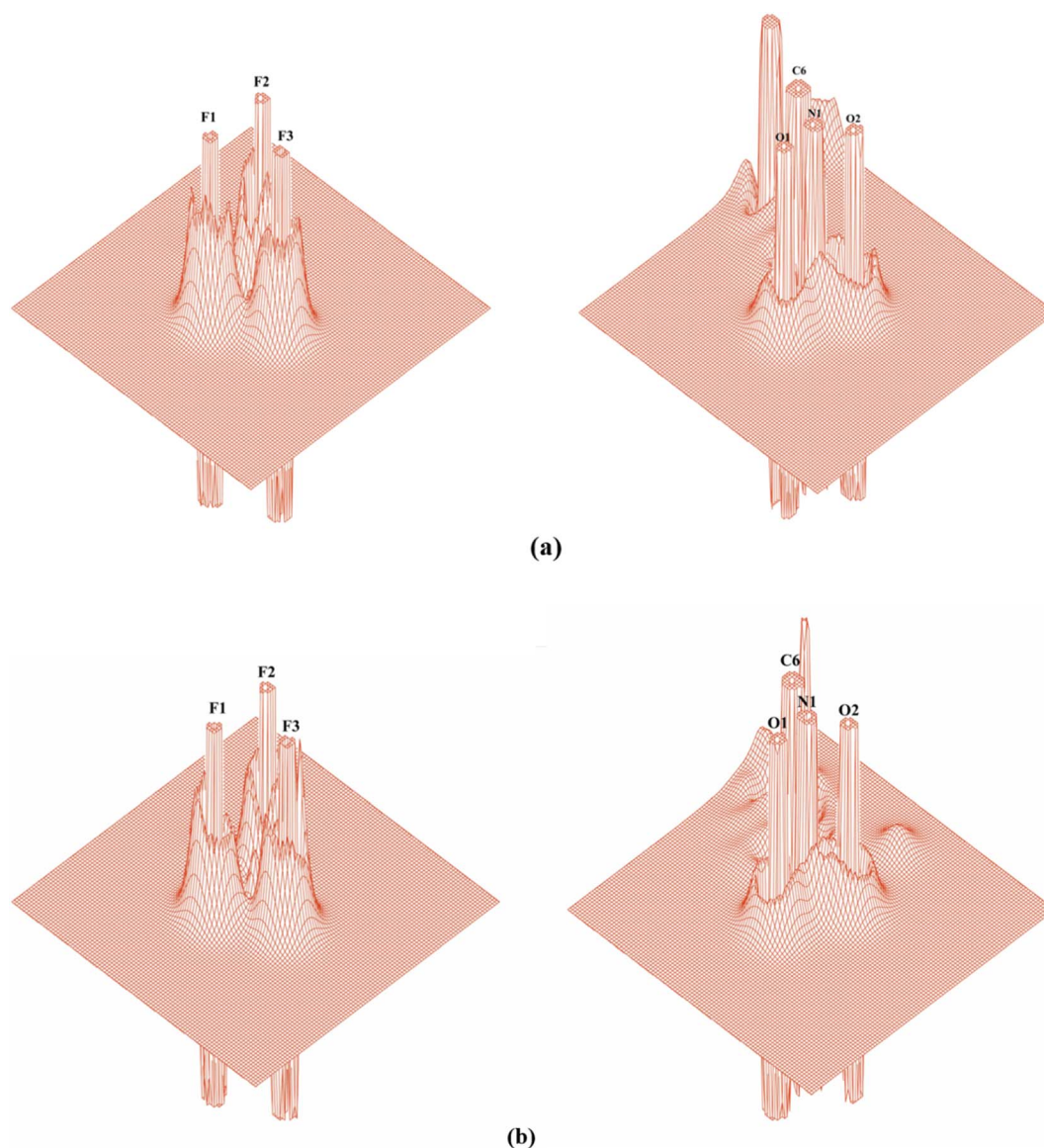**Fig. 8** Relief maps showing the negative Laplacians of electron density (range -50 to $+50$ eÅ^{-5}) of the NO$_2$ and F$_3$ groups of (a) NIL and (b) and FLU molecules.

to the C atoms attached to different groups; these values are found to be significantly higher than the $C_{ar}–C_{ar}$ bonds of the FLU molecule, as the value ranges from -19.258 to -23.148 $e\text{Å}^{-5}$; this indicates that the charges of the $C_{ar}–C_{ar}$ bonds of NIL are less concentrated than in the FLU molecule. The Laplacian of the C–N bonds of the NIL molecule display large variation; the values range from -9.935 to -23.906 $e\text{Å}^{-5}$, in which the C6–N1 (-13.264 $e\text{Å}^{-5}$) and C9–N3 (-9.935 $e\text{Å}^{-5}$) bonds exhibit low values, indicating that the charges of both bonds are depleted in comparison with the other C–N bonds of the NIL molecule. In FLU, the Laplacian of the C8–N2 bond is highly negative and the value is -26.233 $e\text{Å}^{-5}$, indicating that the charges are more highly concentrated than the other non-hydrogen bonds of the molecule; this bonding region is the reactive location and it is prone to electrophilic attack. The Laplacians of the carbonyl bonds C8=O3 and C10=O4 are found to be highly negative and the values are -35.962 and -35.460 $e\text{Å}^{-5}$, respectively, indicating that the charges of these bonds are more highly concentrated than those of the other bonds in the NIL molecule. These are the reactive locations of NIL and FLU molecules, which are prone to electrophilic attack. Whereas the FLU molecule has only one carbonyl bond, C8=O3, and its Laplacian value is much less than that of the NIL molecule, and the value is -13.642 $e\text{Å}^{-5}$; this indicates that the charge concentration is less than that of NIL. The Laplacians of the sp^3 C–C bonds of NIL are almost equal; the average value is -9.651 $e\text{Å}^{-5}$; FLU also maintains a similar trend, but the Laplacian value is slightly higher; the average value is -10.323 $e\text{Å}^{-5}$. The Laplacians of the C_{sp3}–H bonds of NIL are in the range -13.699 to -16.521 $e\text{Å}^{-5}$; whereas in the FLU molecule, these values are relatively higher and are in the range -14.8 to -19.640 $e\text{Å}^{-5}$. In the NIL molecule, the Laplacians of aromatic C–H bonds are in the range -15.888 to -18.580 $e\text{Å}^{-5}$, and are slightly higher than the values of the corresponding bonds of the FLU molecule; the maximum value is -19.899 $e\text{Å}^{-5}$; and these values are also much lower than those for the amino N–H bonds of both molecules, and the values are -27.7 (N3–H3) and -29.221 $e\text{Å}^{-5}$ (N2–H2A). The analysis of the Laplacian of the electron density of both molecules reveals that the charge concentration at the bcp of all the bonds of FLU molecule is relatively less than in the NIL molecule; this may be due to the difference in chemical substituents and the intermolecular interactions in the crystal. The Laplacians of the electron density of both molecules are presented in Table 3. Fig. 7(a and b) show the contour maps of the Laplacians of electron density for NIL and FLU molecules. These shows the lone-pair position (lobes) of the polar O1, O2, O3, O4 atoms of NIL and the O1, O2, O3 atoms of FLU and the F atoms of the CF$_3$ group of both molecules. The relief maps of the Laplacians (Fig. 8(a and b)) of the NO$_2$ and CF$_3$ groups of both molecules also show the lone-pair lobes of both molecules. These lone-pair positions of the respective atoms interact directly with the neighbouring molecules, as described in Section 3.3. These are the locations of electronegative groups which are expected to interact with the complementary electropositive groups present in the active site of the androgen receptor and molecular recognition. The above-mentioned NO$_2$, CF$_3$ and C=O groups are largely involved in interactions and

are correlated with the electrostatic potential described in Section 3.5.

3.3 Topological properties of intermolecular interactions

Topological analysis of electron density at the cps of intermolecular interactions was carried out to understand the strength and nature of the interactions of NIL and FLU molecules present in the crystal. In NIL and FLU molecules, the unit cell packing is stabilized by C–H⋯O, N–H⋯O and C–H⋯F types of intermolecular interaction. The NIL molecule forms hydrogen-bonding interactions (Table 4) with the neighbouring molecules of the crystal. Among all interactions, the N3–H3⋯O3 (x, $1/2 - y$, $-1/2 + z$) interaction is found as a moderate interaction; the calculated electron density and Laplacian of electron density values at the cp of interaction are 0.141 $e\text{Å}^{-3}$ and 2.896 $e\text{Å}^{-5}$, respectively. The molecule also forms C–H⋯O interactions, in which the C1–H1⋯O4 interaction ($1 - x$, $-y$, $-z$) is a weak interaction; the corresponding electron density and the Laplacian of electron density are 0.055 $e\text{Å}^{-3}$ and 0.882 $e\text{Å}^{-5}$, respectively. The C–H group also forms interactions with F atoms; notably, the C–H⋯F type of interaction of both molecules is consistently weak. The electron density and the Laplacian of electron density of the C1–H1⋯F1 ($-x + 1$, $+y + 1/2$, $-z + 1/2 + 1$) interaction of NIL at the cp are 0.037 $e\text{Å}^{-3}$, 0.640 $e\text{Å}^{-5}$, respectively.

The FLU molecule forms an N2–H2A⋯O2 ($-1/2 + x$, $1/2 - y$, $-1 + z$) interaction with the neighbouring molecule; the electron density at the cp of interaction is 0.059 $e\text{Å}^{-3}$, and the Laplacian of electron density is 2.112 $e\text{Å}^{-5}$. In the C4–H4⋯O3 ($1 - x$, $1 - y$, $1/2 + z$) interaction, its electron density and the Laplacian of electron density values are 0.097 $e\text{Å}^{-3}$, 1.385 $e\text{Å}^{-5}$, respectively. Whereas in the C2–H2⋯O1 ($-1/2 + x$, $1/2 - y$, $-1 + z$) interaction, the values are 0.063 $e\text{Å}^{-3}$ and 0.974 $e\text{Å}^{-5}$. The fluorine atoms F1, F2 and F3 of both molecules form C–H⋯F types of interaction in the crystals; notably, all these interactions are found weak compared with the above-mentioned interactions. The cps for all possible interactions were found and the topological parameters were determined (Table 4). The positive Laplacian of electron density of all the interactions indicates that both molecules exhibit a closed shell type of interaction.[52] The topological parameters of intermolecular interactions of NIL and FLU molecules in the crystals are very useful for predicting the strength of NIL/FLU–androgen receptor interactions and recognition (Table 5).

3.4 Gradient vector field and atomic volume

The gradient vector field of electron density is the first derivative of electron density $\nabla\rho(r)$ and it varies at each point of the molecule; it has direction and magnitude. For atoms in the molecule, the gradient trajectory begins at the atom centre and terminates at the bond critical points. The thick solid lines represent the zero-flux surface of atoms in molecule, which define the boundary of the atomic basin. Fig. 9 shows the gradient plots of NIL and FLU molecules. The atomic volumes of O1, O2, O3 and O4 oxygen atoms are higher than those of all other atoms in the molecule; the values are 16.45, 16.98, 18.66,

18.53 Å³, respectively, in which the carbonyl O3 and O4 atoms have slightly more volume than the nitrogen-attached O atoms; the charges of these atoms are −1.12e and −1.13e; whereas the charges of the O1 and O2 atoms are relatively lower and the values are −0.43e and −0.47e, respectively. The volumes of fluorine atoms F1, F2, F3 are 14.37, 14.75 and 14.66 Å³, respectively, and the corresponding atomic charges are −0.62e, −0.69e and −0.73e; these volumes and the charges are much lower than the O atoms. The atomic basins of all F-atoms of both NIL and FLU are drop like in shape. The volumes of N atoms in the molecule are unequal (6.65, 11.50 and 13.66 Å³), as the volume of the N1 atom attached to O atoms is found much lower than those of the N2 and N3 atoms which are attached to C atoms. The atomic basin of all the N atoms has a triangular

Fig. 9 Gradient vector field displaying the atomic basin of each bonded atom in the (a) NIL and (b) FLU molecules.

shape. The integrated charges of N2 and N3 atoms are also found different from that of the N1 atom; the values are −0.99e, −0.90e and 0.51e; the large variation is attributed to highly electronegative atoms attached to the N1 atom. The volume of aromatic C_{ar} atoms ranges from 9.14 to 12.53 Å³; these values are slightly higher than the corresponding C_{ar} atoms of the FLU molecule. The atomic basin of all the C atoms exhibits a triangular shape like N atoms. Notably, the volume of the C7 atom is relatively smaller than those of all other atoms in the molecule; the value is 3.313 Å³. The trend also remains same in the FLU molecule; the theoretical results also predicted the same volume; the low volume may be due to the effect of attached F atoms. The volumes of all other C_{sp3} atoms C9, C11, C12 are 6.08, 9.59, 10.34 Å³, respectively, and a similar trend is also found in the FLU molecule. The volume of aromatic H atoms ranges from 5.72 to 6.18 Å³, whereas that of methyl group H atoms ranges from 5.58 to 6.24 Å³; these volumes are much higher than the H atom of the NH group, whose value is 3.43 Å³. A similar volume can also be noticed in H atoms in FLU, except that a few hydrogens in methyl H atoms show some difference. The gradient vector field in the atomic basin of each H atom differs slightly, however it depends on the attached C or N atom, but the trend remains the same in both molecules. From the above reports, in particular, the carbonyl group O atom exhibits a large volume compared with the other atoms, and the volumes of the atoms in the molecule are in the order O > F > N > C > H (Table 5).

3.5 Electrostatic potential and binding affinity

3.5.1 Electrostatic potential. Fig. 10(a and b) shows the electrostatic potential (ESP) of the NIL and FLU molecules, displaying the electropositive and electronegative regions of the molecules plotted using MolIso software.[53] The ESP of a molecule allows us to predict the binding ability of a molecule with the neighbouring molecules in solids as well as the binding affinity of molecules (ligands) with the active-site residues of proteins.[47,54] The region of positive potential is expected to be the site of electrophilic attack and the region of negative potential that of nucleophilic attack. In NIL, a highly electronegative region is found in the vicinity of NO_2 groups and close to the carbonyl O3, O4 atoms. Similarly, the electronegative region is also present around the fluorine F1, F2 and F3 atoms. A slightly electronegative region is also found in the region of the aromatic ring; this may be due to the π-electron cloud. No negative region is found in the vicinity of the N2 and N3 atoms. The above-mentioned terminal oxygen and fluorine atoms form interactions with the neighbouring complementary charged groups; therefore, these are the important ESP regions for drug binding groups when NIL interacts with the active-site key amino acids of a protein. A similar trend is also found in the FLU molecule; a highly electronegative region is found around the NO_2 group and the carbonyl O3 atom, which is attached to carbon C8 atom. The fluorine atoms F1, F2 and F3 attached to the carbon C7 atom also exhibit an electronegative region, as found in the NIL molecule. An electronegative region found in the region of the aromatic ring is relatively lower than in NIL.
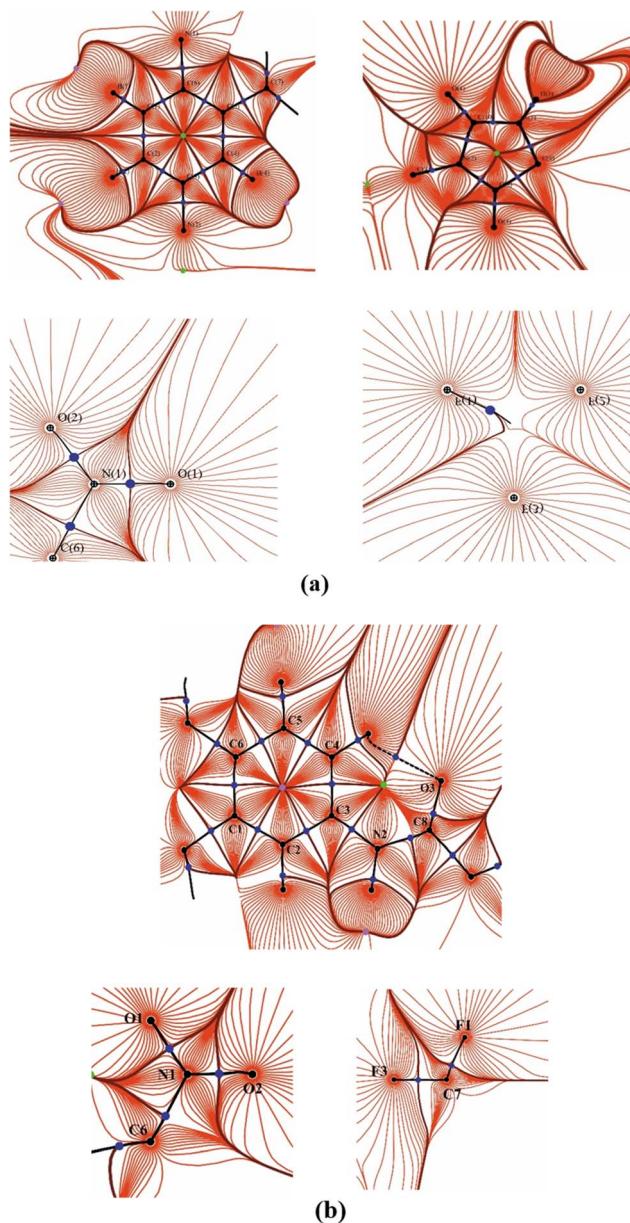
Table 5 Monopole and AIM charges (e), and atomic volumes (Å^3) of (a) nilutamide and (b) flutamide molecules

Atom	Monopole charge	Atomic charge		Volume	
		Experimental	Theoretical	Experimental	Theoretical
(a) Nilutamide					
F1	−0.15	−0.62	−0.39	14.37	13.77
F2	−0.25	−0.69	−0.45	14.75	14.23
F3	−0.19	−0.73	−0.61	14.66	14.12
O1	−0.21	−0.43	−0.40	16.45	16.06
O2	−0.24	−0.47	−0.40	16.98	16.48
O3	−0.29	−1.12	−1.12	18.66	18.43
O4	−0.31	−1.13	−1.00	18.53	17.71
N1	0.24	0.51	0.33	6.65	6.94
N2	−0.29	−0.99	−1.14	11.50	11.64
N3	−0.11	−0.90	−0.94	13.66	13.11
C1	−0.22	−0.16	−0.11	12.53	11.97
C2	−0.22	−0.15	0.07	12.32	11.07
C3	0.14	0.27	0.30	9.14	9.09
C4	−0.22	−0.10	0.07	11.70	10.94
C5	−0.05	−0.11	−0.02	10.28	9.38
C6	−0.08	0.06	0.20	9.71	9.48
C7	0.23	1.69	2.01	3.13	2.97
C8	0.28	1.37	1.35	5.47	5.24
C9	−0.07	0.16	0.22	6.08	5.83
C10	0.24	1.62	0.75	5.31	6.87
C11	−0.10	0.08	−0.05	9.59	9.69
C12	−0.15	−0.01	0.05	10.34	9.35
H1	0.17	0.16	0.21	5.45	5.72
H2	0.20	0.18	0.07	5.75	6.18
H4	0.18	0.18	0.09	4.98	5.77
H3	0.26	0.49	0.49	3.43	3.05
H11A	0.20	0.12	0.06	6.42	6.24
H11B	0.22	0.18	0.09	5.54	5.69
H11C	0.19	0.13	0.08	6.10	5.58
H12A	0.20	0.14	0.06	6.11	5.81
H12B	0.19	0.15	0.04	5.85	6.15
H12C	0.20	0.16	0.05	5.93	5.90
(b) Flutamide					
F1	−0.27	−0.92	−0.59	14.86	14.26
F2	−0.20	−0.92	−0.63	15.10	14.58
F3	−0.15	−0.75	−0.58	14.36	14.27
O1	−0.29	−0.50	−0.37	16.86	16.09
O2	−0.31	−0.51	−0.45	16.28	15.74
O3	−0.29	−0.14	−1.17	18.52	17.50
N1	0.34	0.54	0.31	7.32	7.32
N2	−0.25	−1.40	−1.00	14.72	13.30
C1	0.05	0.24	0.09	8.17	9.43
C2	−0.29	−0.07	−0.05	10.82	11.01
C3	−0.09	0.07	0.30	10.00	8.98
C4	−0.30	−0.05	−0.002	11.51	11.43
C5	−0.33	−0.19	−0.001	11.78	11.10
C6	0.34	0.30	0.21	10.19	9.72
C7	0.15	2.10	1.52	2.80	3.63
C8	0.27	1.38	1.28	5.33	5.00
C9	0.10	0.37	0.17	6.68	6.56
C10	−0.28	−0.15	−0.07	10.60	9.91
C11	−0.27	−0.39	−0.10	12.75	10.07
H2	0.29	0.11	0.10	6.63	5.91
H4	0.38	0.27	0.19	5.23	4.90
H5	0.37	0.30	0.13	5.04	5.69
H2A	0.25	0.52	0.40	2.49	3.72
H9	0.22	0.07	−0.02	6.53	6.31
H10A	0.20	0.19	0.08	5.42	5.78
H10B	0.09	0.03	0.01	5.75	6.06

Table 5 (*Contd.*)

Atom	Monopole charge	Atomic charge		Volume	
		Experimental	Theoretical	Experimental	Theoretical
H10C	0.10	0.01	0.06	7.07	6.02
H11A	0.27	0.27	0.008	5.08	6.08
H11B	0.20	0.18	0.08	5.60	5.82
H11C	0.24	0.31	0.08	3.66	5.87

Although the above-mentioned groups are structurally identical in both molecules, the strength of the ESP regions between the molecules differ in magnitude, as FLU has more highly electronegative regions than NIL. Overall, the calculated minimum (V_{min}) and maximum (V_{max}) values of the ESP of NIL are -0.192, 0.35 e Å^{-1}, respectively; whereas the values of ESP of FLU are -0.218 and 0.742 e Å^{-1} (Fig. 10(a and b)). The ESP values of the FLU molecule are relatively higher than those of the NIL molecule, revealing that FLU may interact strongly with the androgen receptor; however, it also depends on the specific drug–androgen interactions in the binding pocket.

3.5.2 Molecular docking analysis. The docking analysis reveals that the maximum docking score values of NIL and FLU ligands with an androgen receptor protein are -9.1 and -8.7 kcal mol^{-1}, respectively (Table S1). Fig. 10(c and d) shows the interactions of NIL and FLU molecules with the active-site amino acid residues of the androgen receptor protein. The O1 and O2 are the electronegative atoms of the NIL molecule, in which the O1 atom forms a hydrogen-bonding interaction with ARG752 at a distance of 2.78 Å and the O2 atom also forms a hydrogen-bonding interaction with ARG752 at a distance of 2.72 Å (Fig. 10). Whereas in FLU, the O1 and O2 atoms form O1···GLN711 and O2···GLN711 interactions at distances of 3.06, 2.43 Å, respectively. Further, the O2 atom also forms another interaction O2···ARG752 at a distance of 2.75 Å. The fluorine atom F1 of NIL interacts with MET745, forming an F1···MET745 interaction at a distance of 3.19 Å; whereas in FLU, the F2 atom interacts with MET745, forming an interaction F2···MET745 at a distance of 3.34 Å. In NIL, the electropositive atom H3 interacts with ASN705, forming an interaction H3···ASN705 at a distance of 1.878 Å; whereas in FLU, the electropositive atom H3A interacts with the LEU704 residue, forming an interaction H3A···LEU704 at a distance of 3.04 Å. The carbonyl oxygen atom O4 interacts with GLY708, forming an interaction O4···GLY708 at a distance of 3.46 Å and no other carbonyl oxygen atoms of either molecule interact with the active-site amino acids of the androgen receptor. In both molecules, the formation of pi···pi interactions is also observed (Tables S2a and b). Overall, both ligands are structurally related; however, the FLU lacks the imidazalone ring found in NIL. The docking analysis reveals that the structural difference does not influence the interaction much. This can be well understood from the interaction of NIL with androgen; the interacting residues are ARG752, ASN705, GLN711, GLY708 and MET745, among which ARG752, ASN705, and GLN711 are key polar residues that form

hydrogen bonds with the androgen. These interactions are predominant in the hydrophobic binding pocket, which are crucial for the function of NIL as a non-steroidal antiandrogen used in prostate cancer treatment.

Whereas FLU interacts with ARG752, GLN711, LEU704 and MET745. Both molecules interact with the key amino acids of the androgen receptor. The interaction between NIL/FLU molecules and the androgen receptor are listed in Table S2b.

3.5.3 Approximation and transfer of electrostatic potential. The ESP of both molecules at the binding site of the androgen is related directly to the binding affinity. Experimentally, exploring the ESP of a drug molecule and interactions at the binding pocket of a protein using charge density analysis is not straightforward; this is due to the experimental and computational challenges associated with obtaining and refining high-resolution X-ray diffraction data for large complex biological molecules.[55] Therefore, an approximation of the ESP of NIL/PLU molecules obtained from the crystal environment was used as an approximation for the ESP of NIL/FLU at the active site of the androgen receptor. In this approximation, potentially interacting atoms within the drug's crystal structure were identified. Subsequently, molecular docking analysis was employed to assess whether these atoms interact with the active site amino acids of androgen. If these interacting atoms of the crystal could form interactions with the active-site amino acids of the androgen, then the ESP of interacting atoms in the crystal is approximated as the ESP of those same atoms while interacting with the active site amino acids of the androgen receptor. To accomplish this, here we performed the above-mentioned molecular docking simulation of NIL and FLU with the androgen receptor protein[56] and approximated the ESP of interacting atoms of NIL/FLU in the crystal with the ESP of the same interacting atoms of NIL/FLU in the active site of the androgen receptor.

Electrostatic potential relates directly to intermolecular interactions in molecular docking by predicting and quantifying the electrostatic forces that govern how molecules recognize and bind to each other. A favourable docking pose is characterized by complementary electrostatic potential surfaces. Therefore, here we relate the experimental ESP of NIL/FLU and the interactions predicted from the molecular docking simulation. Furthermore, it can be predicted how the atoms with negative/positive ESP regions of these ligands when interact with the amino acids of the active site of the androgen receptor. Based on the docking study and experimental ESP, it is
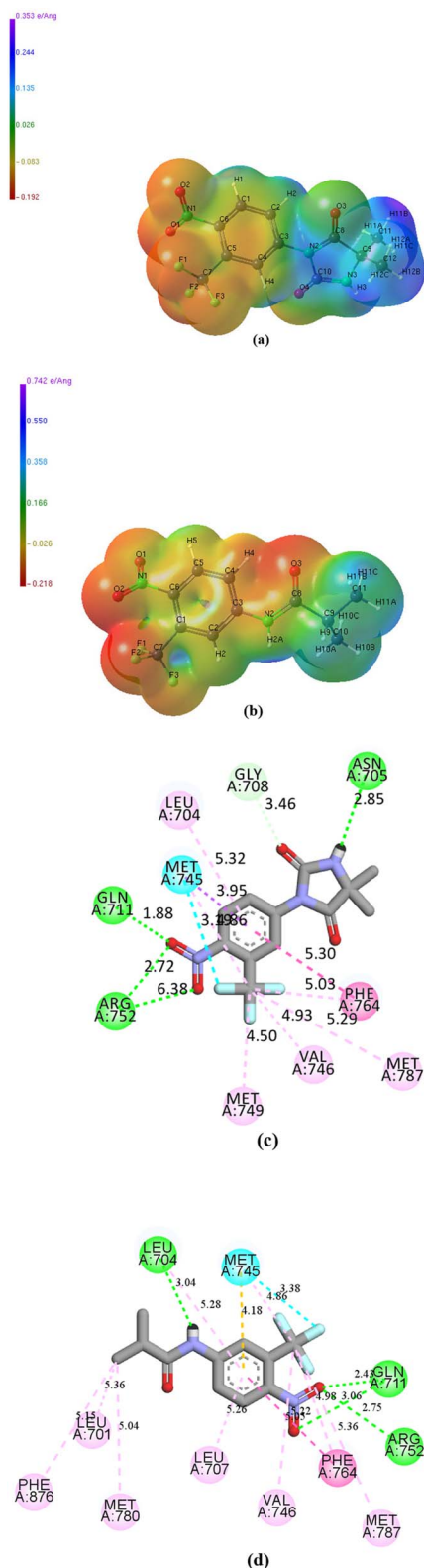
Fig. 10 Experimental ESP maps of (a) the NIL molecule showing ESP with $V_{min} = -0.192$ e Å^{-1} and $V_{max} = 0.35$ e Å^{-1} and (b) the FLU molecule with $V_{min} = -0.218$ e Å^{-1} and $V_{max} = 0.742$ e Å^{-1}. The intermolecular interactions of (c) NIL and (d) FLU with the active-site amino acids of the androgen receptor obtained from the molecular docking simulation.

found that the experimentally observed electronegative ESP of O1 and O2 atoms of NIL interact strongly with ARG752 and GLN711 amino acids; whereas in FLU, the electronegative region of ESP of O1 and O2 atoms also interact strongly with ARG752 and GLN711 amino acids. The electronegative ESP region of the F1 atom of NIL potentially interacts with MET745 amino acid; whereas in FLU, the electronegative ESP of F2 interacts with MET745. The highly electropositive ESP of the H3 atom of NIL interacts with ASN705 amino acid; whereas in FLU, the electropositive ESP region of the H2A atom interacts with the LEU704 amino acid of the androgen receptor. In NIL, the electronegative ESP of the carbonyl O4 atom also interacts with GLY708 amino acid; although the electronegative ESP is found in the vicinity of the carbonyl O3 atom of FLU, no interactive location is found at the active site of the androgen. From the above, we understand that the electronegative ESP regions of the ESP of O1, O2, O3, O4, F1 and the electropositive region of H3 atoms interact with the amino acids ARG752, ASN705, GLN711 GLY708 and MET745 present in the active site of the androgen receptor (Table S2a). Whereas in FLU, the electronegative ESP region of O1, O2, O3, F2 and the electropositive region of H2A atoms interact with the amino acids ARG752, GLN711, LEU704 and MET745 (Table S2b). From the above, it can be confirmed that the atoms of NIL/FLU drugs potentially interact, when they bind with the androgen receptor. However, the difference in ESP is explicitly reflected in the interactions and recognition. This relative study approximates the ESP of both molecules when situated in the binding pocket of the androgen receptor by forming interactions to the ESP of same molecules in the crystal environment derived from the experimental charge density.

4   Conclusion

A high-resolution X-ray experiment and theoretical charge density analysis of both molecules reveal that the charge density $\rho_{bcp}(r)$ at the bcp of bonds shows charge accumulation. The Laplacian of electron density $\nabla^2\rho_{bcp}(r)$ identifies charge concentration and depletion at the bcp of bonds; if the value is negative, then the charges are concentrated and the bonding exhibits a shared interaction: then such bonds are covalent bonds; whereas positive values indicate that the charges are depleted, confirming that it is a closed-shell interaction, which is either ionic or non-covalent bonding. The comparison of the topological properties of the electron density of experimental and theoretical studies of NIL and FLU shows the effect of the crystal field in the chemical bonding of a crystal. The charge density $\rho_{bcp}(r)$ values of N–O bonds of the NO$_2$ group of both NIL and FLU molecules are almost at same at $\sim$3.3 eÅ^{-3} and the Laplacian value of NIL is $\sim$−12.9 eÅ^{-5}, whereas in FLU, the value of one of the N–O bonds is found to be lower. In the C–F bonds of NIL, the average electron density is 1.895 eÅ^{-3}, which is slightly lower than in FLU where the value is 1.922 eÅ^{-3}. Among the Laplacians of the C–F bonds of NIL, the value of C7–F3 is −22.05 eÅ^{-5}, which is much higher than those of the C–F bonds of FLU where the maximum value is −18.98 eÅ^{-5}. The carbonyl C═O bond of NIL is $\sim$3.0 eÅ^{-3}, which is slightly higher than the same value in FLU, which is $\sim$2.9 eÅ^{-3}. The Laplacian of C═O

bonds of NIL is ~-35.0 e$Å^{-5}$, which is significantly higher than that of the C8=O3 bonds of FLU, indicating that the charges are highly concentrated, which is the reactive location (C8) of the NIL molecule. Relatively, the charge accumulation and charge concentration at the bcp of NIL bonds is higher than in FLU. Overall, the charge density of both molecules significantly influences their different electrostatic potentials, which decides the binding affinity of both molecules towards the androgen receptor, mediated by electrostatic interactions.

The docking analysis reveals that the structural difference between the molecules influences their interaction with the androgen receptor and shows their differences. In NIL–androgen interactions, the O1, O2, O3, O4, F1 and H3 atoms interact with ARG752, ASN705, GLN711 GLY708 and MET745; whereas in FLU–androgen, the O1, O2, O3, F2 and H3A atoms interact with ARG752, GLN711, LEU704 and MET745. The ESP derived from the experimental charge density of NIL and FLU molecules exhibits a high value in the vicinity of the polar atoms of NO_2, CF_3, C=O and NH groups atoms, which form interactions with the neighbours in the crystals. The docking study also predicts that these atoms are involved in drug–androgen interactions. Visually, NIL exhibits a higher ESP surface (Fig. 10(a and b)) than FLU as well as more interactions, which confirms that NIL has higher binding ability than FLU. The ESP of the interacting groups of both molecules in the active site of androgen receptor is approximated to the ESP of the same in the same molecular environment of crystal. In both molecules, the CF_3 functional group may be replaced by other functional groups to form a strong interaction with the androgen receptor. The strong ESP of the NO_2 group indicates its highly reactive nature; therefore, this group may be replaced with a suitable functional group to reduce the hepatoxicity caused by both molecules. Overall, the fine structural details derived at electronic level from the high-resolution experiment and theoretical study will provide useful insights to redesign both molecules for improved binding and to alleviate potential side effects.

Author contributions

Hemalatha Balasubramanian – designed the study, data analysis and interpretation and wrote the manuscript. Saravanan Kandasamy – helped with the SuperNova HyPix detector fitted diffractometer data collection. Venkatesha R Hathwar – helped with the theoretical Crystal09 calculations. Rajesh G. Gonnade – helped with the BRUKER D8 Venture with PHOTON III detector diffractometer data collection. Kumaradhas Poomani – supervised and revised the manuscript.

Conflicts of interest

There are no conflicts to declare.

Data availability

CCDC 2491318 and 2491319 contain the supplementary crystallographic data for this paper.[57a,b]

The authors declare that the data supporting the findings of this study are available within the paper and its supporting supplementary information (SI). Supplementary information is available. See DOI: https://doi.org/10.1039/d5ra07636f.

References

1 H. E. Taitt and Am. J. Mens, *Health*, 2018, **12**, 1807–1823.
2 M. Sekhoacha, K. Riet, P. Motloung, L. Gumenku, A. Adegoke and S. Mashele, *Molecules*, 2022, **27**, 1–33.
3 T. K. Wilson and O. T. Zishiri, *Cancer Rep.*, 2024, 7(10), e70016.
4 M. Namer, *J. Steroid Biochem.*, 1988, **31**, 719–729.
5 P. Reid, P. Kantoff and W. Oh, *Invest. New Drugs*, 1999, **17**, 271–284.
6 M. Rashid, K. Shamshavali and M. Chhabra, *Curr. Clin. Pharmacol.*, 2019, **14**, 108–115.
7 S. Student, T. Hejmo, A. Poterała-Hejmo, A. Leśniak and R. Bułdak, *Eur. J. Pharmacol.*, 2020, **866**, 172783.
8 S. M. Singh, S. Gauthier and F. Labrie, *Curr. Med. Chem.*, 2000, **7**, 211–247.
9 S. Takegami, K. Kitamura, M. Ohsugi, A. Konishi and T. Kitade, *AAPS PharmSciTech*, 2016, **17**, 1500–1506.
10 C. E. Bohl, D. D. Miller, J. Chen, C. E. Bell and J. T. Dalton, *J. Biol. Chem.*, 2005, **280**, 37747–37754.
11 T. Koritsanszky, *Acta Crystallogr. Sect. A Found. Crystallogr.*, 1998, **54**, 686.
12 D. Stalke, *Chem.–A Eur. J.*, 2011, **17**, 9264–9278.
13 N. S. Trasi, P. E. Fanwick and L. S. Taylor, *Acta Crystallogr., Sect. E:Struct. Rep. Online*, 2012, **68**, 0591–0591.
14 J. M. Cense, V. Agafonov, R. Ceolin, P. Ladure and N. Rodier, *Struct. Chem.*, 1994, **5**, 79–84.
15 *Rigaku Oxford Diffraction: SuperNova X-ray diffractometer*, Rigaku Corporation, Tokyo, Japan, 2015.
16 *Rigaku Oxford Diffraction: Crys Alis Pro*, Rigaku Corporation, Tokyo, Japan, 2015.
17 R. H. Blessing, *J. Appl. Crystallogr.*, 1997, **30**, 421–426.
18 W. Madison, Bruker D8 Venture diffractometer, *Bruker AXS Inc.*, 2001.
19 W. Madison, APEX3, Bruker AXS Inc., 2015.
20 W. Madison, SAINT, Bruker AXS Inc., 2012.
21 W. Madison, SADABS, Bruker AXS Inc., 2001.
22 L. J. Farrugia, *Data Reduction using SORTAV Analysis Tutorial 2*, 2007, pp. 1–11.
23 G. M. Sheldrick, *Acta Crystallogr., Sect. C:Struct. Chem.*, 2015, **71**, 3–8.
24 L. J. Farrugia, *J. Appl. Crystallogr.*, 2012, **45**, 849–854.
25 A. Volkov, T. Koritsanszky, P. Macchi, C. Gatti, L. J. Farrugia and P. R. Mallison, A computer program package for multipole refinement and analysis of charge densities from diffraction data, *XD2016*, 2016.
26 N. K. Hansen and P. Coppens, *Acta Crystallogr., Sect. A*, 1978, **34**, 909–921.
27 P. S. V. Kumar, V. Raghavendra and V. Subramanian, *J. Chem. Sci*, 2016, **128**, 1527–1536.
28 A. O. Madsen, *J. Appl. Crystallogr.*, 2006, **39**, 757–758.
29 R. F. W. Bader, *Chem. Rev.*, 1991, **91**, 893–928.

30 R. F. W. Bader, *Atoms in Molecules – A Quantum Theory*, Oxford University Press, 1990.

31 R. J. Gillespie and P. L. A. Popelier, *Chemical Bonding and Molecular Geometry: from Lewis to Electron Densities, Oxford University Press*, Oxford University Press, 2001.

32 Y. A. Abramov, *Acta Crystallogr., Sect. A:Found. Crystallogr.*, 1997, **53**, 264–272.

33 R. Dovesi, V. R. Saunders, C. Roetti, R. Orlando, F. Pascale, B. Civalleri, K. Doll, N. M. Harrison, I. J. Bush, M. Llunell and C. Science, *A. Technologies Crystal09 - User's Manual*, 2013, pp. 1–307.

34 A. D. Becke, *J. Chem. Phys.*, 1993, **98**, 5648–5652.

35 H. Su, G. Ma and Y. Liu, *Inorg. Chem.*, 2018, **57**, 11738–11745.

36 J. A. Frisch, M. J.; G. W. Trucks; H. B. Schlegel; G. E. Scuseria; M. A. Robb; J. R. Cheeseman; J. A. Montgomery; T. Vreven; K. N. Kudin; J. C. Burant; J. M. Millam; S. S. Iyengar; J. Tomasi; V. Barone; B. Mennucci; M. Cossi; G. Scalmani, *Gaussian03*, Inc, 2004.

37 J. Eberhardt, D. Santos-Martins, A. F. Tillack and S. Forli, *J. Chem. Inf. Model.*, 2021, **61**, 3891–3898.

38 O. Trott and A. J. Olson, *J. Comput. Chem.*, 2010, **31**, 455–461.

39 PyMOL, *Molecular Graphic System, Ver. 3.0*, Schrodinger LLC, 2024.

40 U. Baroroh, S. Si., M. Biotek., Z. S. Muscifa, W. Destiarani, F. G. Rohmatullah and M. Yusuf, *Indones. J. Comput. Biol.*, 2023, **2**, 22.

41 L. J. Farrugia, *J. Appl. Crystallogr.*, 2012, **45**, 849–854.

42 A. L. Spek, *J. Appl. Crystallogr.*, 2003, **36**, 7–13.

43 M. Nardelli, *J. Appl. Crystallogr.*, 2021, **45**, 849–854.

44 P. R. Spackman, M. J. Turner, J. J. McKinnon, S. K. Wolff, D. J. Grimwood, D. Jayatilaka and M. A. Spackman, *J. Appl. Crystallogr.*, 2021, **54**, 1006–1011.

45 V. R. Hathwar and T. N. G. Row, *Cryst. Growth Des.*, 2011, 1338–1346.

46 C. Kalaiarasi, M. Sivanandam, S. Suganya, G. Christy, R. G. Gonnade, V. R. Hathwar and P. Kumaradhas, *J. Mol. Struct.*, 2020, **1220**, 128714.

47 G. Rajalakshmi, M. S. Pavan and P. Kumaradhas, *RSC Adv.*, 2014, **4**, 57823–57833.

48 G. Rajalakshmi, V. R. Hathwar and P. Kumaradhas, *Acta Crystallogr., Sect. B:Struct. Sci., Cryst. Eng. Mater.*, 2014, **70**, 568–579.

49 G. Rajalakshmi, V. R. Hathwar and P. Kumaradhas, *Acta Crystallogr. Sect. B Struct. Sci. Cryst. Eng. Mater.*, 2014, **70**, 331–341.

50 E. A. Zhurova, C. F. Matta, N. Wu, V. V. Zhurov and A. A. Pinkerton, *J. Am. Chem. Soc.*, 2006, **128**, 8849–8861.

51 A. A. Korlyukov, M. Malinska, A. V. Vologzhanina, M. S. Goizman, D. Trzybinski and K. Wozniak, *IUCrJ*, 2020, **7**, 71–82.

52 A. Iruthayaraj, K. Chinnasamy, K. K. Jha, P. Munshi, M. S. Pavan and P. Kumaradhas, *J. Mol. Struct.*, 2019, **1180**, 683–697.

53 C. B. Hubschle and P. Luger, *J. Appl. Crystallogr.*, 2006, **39**, 901–904.

54 A. Hasil, A. Mehmood, S. Noureen and M. Ahmed, *J. Mol. Struct.*, 2020, **1216**, 128295.

55 K. Florian, W. Erna K., H. Emanuel, W. S. Ming, S. Scott G., J. Dylan, T. Michael J., S. Kunihisa, N. Eiji, S. Tanja, S. Thomas C., E. Bernd and G. Simon, *Chem.–Eur. J.*, 2021, **27**, 3407–3419.

56 A. K. Gupta, Y. Sahu, D. Pal, N. Kumar and S. K. Jain, *Comput. Biol. Chem.*, 2025, **117**, 108424.

57 (*a*) CCDC 2491318, Experimental Crystal Structure Determination, 2025, DOI: 10.5517/ccdc.csd.cc2pmf3w; (*b*) CCDC 2491319, Experimental Crystal Structure Determination, 2025, DOI: 10.5517/ccdc.csd.cc2pmf4x.